A theoretical Model for Flow about a circular-arc Aerofoil with Separation

Thesis by
Stéphane Cyr

Department of Mechanical Engineering
McGill University, Montréal, Canada.

Submitted March 1992

Thesis submitted to the Faculty of Graduate Studies and Research
in partial fulfillment of the requirements for the degree of
Master's of Engineering.

A mes parents,
Jacques et Estelle

Abstract

An important problem in aerodynamics is the prediction of separation on aerofoils. On sails, where leading-edge and trailing-edge separations are usually present at the same time, the prediction is even more complicated because the presence of separation influences the shape of the sail. In an attempted to know more about aerodynamics of sails, the interesting problem of trailing-edge separation is considered. It is possible to study the isolated phenomena by removing the flexibility of the sail and by choosing the angle of attack such that only the trailing-edge separation is present.

The aim of the present research is to develop a theoretical model that could predict the trailing-edge separation over a circular-arc aerofoil and its effect on the pressure distribution, and on the lift. The model uses sources, in a potential flow, to simulate the effect of the separated region on the pressure distribution. An integral method, turbulent boundary-layer development, combined with the irrotational pressure distribution on the circular-arc predicts the point of separation. The strength and the distribution of the sources are then modified until a set of closure conditions is satisfied These closure conditions are chosen to make the flow around the aerofoil as realistic as possible. To make sure that trailing-edge separation is present alone and mostly to avoid any difficulties in predicting the boundary-layer flow after reattachment, the aerofoil is studied at design incidence.

Two different circular-arc aerofoils were tested; one of 10% and one of 18% camber. The calculation for the 10% aerofoil did not predict any separation at design incidence, which was confirmed experimentally. The theoretical model predicted the right position of separation for the 18% aerofoil. It also provided a good simulation of the pressure distribution, including the right value for the

i

base pressure and a good prediction of the lift. It follows that the pressure distribution when integrated, gives a good estimate of the pressure or form drag.

This research is a preliminary investigation to show that sources in potential flow combined with a boundary-layer calculation method and plausible closure conditions, seem to be able to predict adequately the trailing-edge separation on aerofoils and its effect. Validation of the theoretical closure conditions depends partly on the measurements on the 18% aerofoil and thus, strictly speaking, the numerical method has not been verified for other camber ratios. However, there is no serious reason to suggest that the predictions will be seriously in error.

Simulations of other kinds of aerofoil will eventually be done to verify the general applicability of the method. This approach could also be used to simulate the effect of a trailing-edge separation on sails.

Résumé

Un important problème en aérodynamique est la prédiction de la séparation sur un profils d'aile. Sur une voile, la prédiction de la séparation est encore plus difficile car les zones de séparations, qui peuvent être présentes au bord d'attaque et au bord de fuite en même temps, influencent la forme que prendra la voile. Dans le but d'en savoir un peu plus sur l'aérodynamique des voiles, le problème de la séparation au bord de fuite est considéré. En éliminant la flexibilité de la voile et en choisissant un angle d'attaque tel que seule la séparation au bord d'attaque est présente, il est possible d'étudier la séparation de façon isolé et simplifié.

Le but de la présente recherche est de développer un modèle théorique qui puisse prédire la séparation au bord de fuite d'un profil d'arc circulaire et l'effet de celle-ci sur la distribution de pression et la portance. Le modèle utilise l'implantation de sources dans l'écoulement potentiel pour simuler l'effet de la séparation sur la distribution de pression. La distribution de pression obtenue est utilisée dans un calcul de développement de couche limite turbulente pour prédire la position du point de séparation. La puissance et la distribution des sources sont ensuite modifiées jusqu'à ce qu'un ensemble de conditions de fermeture soit satisfait. Ces conditions de fermeture sont choisies pour rendre l'écoulement autour du profil d'aile aussi réaliste que possible. Pour éviter toute complications dans le calcul de couche limite dû à la présence de bulles de séparation au bord d'attaque du profil, celui-ci est étudié au "design incidence".

Deux profils d'arc différents ont été étudiés, un premier à 10% et un autre à 18% de cambrure. La simulation de l'écoulement autour du profil à 10% ne prédit aucune séparation, ce qui est vérifié expérimentalement. Le modèle théorique prédit la bonne position de séparation pour le profil à 18% de cambrure.

Il simule aussi très bien la distribution de pression autour du profil, incluant la bonne prédiction de la pression de base et une bonne évaluation de la portance. Il en résulte que la distribution de pression obtenue, une fois intégrée, donne une bonne évaluation de la traînée due à la pression.

Cette recherche se veut une étude préliminaire pour démontrer que l'utilisation de sources dans un écoulement potentiel combinée à un calcul de développement de couche limite semble permettre, en conjonction avec un ensemble de conditions de fermeture plausibles, de prédire adéquatement la séparation de l'écoulement au bord de fuite d'un profil d'aile. La validation des conditions de fermeture dépend en partie des résultats expérimentaux obtenues sur le modèle de 18% de cambrure. Donc, strictement parlant, la méthode numérique n'a pas été vérifiée pour d'autres cambrures. Cependant, aucune raison apparente ne permet de douter de l'applicabilité de la méthode à d'autres arcs de cercle.

La simulation d'autres profils d'aile sera effectuée pour vérifier l'applicabilité générale du modèle théorique. L'approche utilisée pourra aussi être étendue à la simulation de l'effet de la séparation au bord de fuite d'une voile.

Acknowledgments

I sincerely thank my supervisor, Dr. B. G. Newman, for his direction and guidance and for the confidence he showed, by providing me with financial support for this research.

Many thanks goes to Steve Markhauser, Senior Technician in the Aerodynamics Laboratory, for his excellent job in constructing the experimental models.

I must also thank Victor Storm and John Saabas for the several hours past discussing turbulence, fluid mechanics and not always related topics; and the students of room 368 for the good working atmosphere and for the mutual help.

Finally I would like to show my gratitude to Josiane for her patience and her understanding.

Table of Contents

List of Figures

Nomenclature

Greek Symbols

α Angle of attack

Δ Total length of distribution of sources

δ Polar position of the point source on the circular cylinder

δ_1 Starting position of the distribution of sources

δ_2 Ending position of the distribution of sources

δ^* Displacement thickness

ϵ Offset alignment between the aerofoil and the balance

Γ Strength of the central vortex (circulation)

ς Dimensional complex variable in the circular-arc plane

θ Momentum thickness or dummy polar angle

ρ Fluid density

σ Distribution of the strength of the sources in the circle plane

τ Polar position of the point that mappes to the trailing edge

Roman Symbols

a	Radius of the transformation circle
b	Radius of the circular cylinder
C	Chord
C_d	Drag coefficient
C_l	Lift coefficient
C_p	Pressure coefficient
C_{pm}	Modified pressure distribution
c	Offset distance between the centers of the circular cylinder and the transformation circle
D	Drag
$F(z)$	Complex potential
H	Shape factor δ^*/θ
L	Lift
M	Point source strength
m	Constant source strength / unit length
p	Pressure
Re	Reynolds number $\rho U C/\mu$
U	Free-stream velocity
u	X-coordinate velocity
v	Y-coordinate velocity
$W(z)$	Complex velocity
X	Force component approx. aligned with the chord
x'	Axes direction align with the free-stream velocity
Y	Force component approx. perpendicular to the chord
y'	Axes direction perpendicular to the free-stream velocity
z	Dimensional complex variable in the circular cylinder plane
z_1	Dimensional complex variable alingned with the free-stream flow

Chapter 1

Introduction

An important problem in the simulation of flow past aerofoils, is the prediction of flow separation. Flow separation over aerofoils is a condition that is associated with the stall. The maximum lift coefficient of an aerofoil is, by definition, at the stall, and this value is of prime importance to aerodynamicists. Therefore, there is a need for numerical methods that would take into account possibly large regions of flow separation and provide the characteristics of the aerofoil near the stall.

A sail is also a lifting surface over which separation can occur. On top of the possible presence of a trailing-edge separation, the sharp leading-edge of a sail can generate large pressure gradients that makes the flow separate to form a leading-edge bubble [9]. Hence on a sail, two regions of separation can be present at the same time. In aerodynamics of sails, it is important to be able to determine the pressure distribution on a given shape of sail, because determining the final shape of the sail is a non-linear problem. The shape of the sail changes the pressure distribution and the pressure distribution changes the shape of the sail until equilibrium between the aerodynamic load and the tension in the sail. The aerodynamic load is very dependent on the presence

of separated regions. So in order to eventually develop a numerical model that would predict the aerodynamic performances of sails, it is important to be able to incorporate the effect of large regions of separation in the flow field around the sail. To understand how the effect of the leading-edge or the effect of the trailing-edge can be simulated, basic studies of these phenomena are necessary.

Leading-edge bubbles are not phenomena that are exclusive to sails. They can be found on practically any aerofoils but they are more likely to be found on aerofoils with sharp leading-edges. Newman and Tse [8] have worked on the simulation of leading-edge bubbles on a flat plate. On such a plate, there is only leading-edge separation present for any angle of attack below 8° and the phenomenon is isolated. In potential flow, they used a uniform distribution of sources to simulate the entrainment of the main flow in the leading-edge bubble and a weaker distribution of sources was used on the remaining surface of the plate to simulate the skin friction drag. The wake thickness produced by the sources was then used with the assumption that in the far wake the displacement thickness is nearly equal to the momentum thickness. The drag was found using the approximated momentum thickness. By associating the lost of leading-edge suction with the drag on the plate, they were able to correlate the size of the leading-edge bubble with the angle of attack. The use of sources to simulate the drag goes at least as far back as Prandtl [13]. G.I. Taylor [16] also used sources to simulate the drag of a flat plate of very porous material mounted at right angles to the flow. Using potential flow theory, the plate was represented by a series of point sources. With the argument mentioned above concerning the momentum thickness, he was able to estimate the drag of the plate.

A logical extension to the work of Newman and Tse, was to consider the investigation of the effect of trailing-edge separation. Bearing in mind the problem of flow separation on sails, the present investigation was conceived. Some simplifications of the problem of the sail are considered to focus the

2

investigation on the simulation of the effect of trailing-edge separation alone. The study of an air flow over a rigid circular-arc aerofoil is considered. It has the advantage of removing the problem of the flexibility of the sail and the arc approximates the shape of a sail. To study the effect of trailing-edge separation alone, it was decided to study the circular-arc at design incidence. At this angle of attack no leading-edge bubbles are formed.

In Newman's approach to treat the leading-edge separation, sources are used in potential flow to simulate the effect of the leading-edge bubble. The sources are implanted near the leading-edge of the flat plate to provide some blockage to the main flow, therefore eliminating the leading-edge suction. These sources are simulating the entrainment found in a real separation bubble. Because the velocity profile in a separation bubble is similar (except the back flow part) to the velocity profile of a turbulent mixing layer, the entrainment in the bubble is assumed to be similar to the entrainment in a mixing layer. The growth of a turbulent mixing layer is linear with distance so a constant entrainment in the mixing region is found and hence a constant distribution of sources is used on the flat plate. The good agreement obtained between the simulation of the drag and the experimental results for the flat plate is an indication that a continuous distribution of sources is able to simulate the effect of separation. Hence the same arguments were used to approach the simulation of the trailing-edge separation. The basic idea was to implant a continuous distribution of constant sources near the trailing-edge of a circular-arc aerofoil, in potential flow. This is again to simulate the entrainment in the separated region due to the free shear layer.

If sources are implanted on the extrados of an aerofoil near the trailing-edge, it can be noticed that they modify the pressure distribution ahead of them. In a real flow, a separated region has a large influence on the pressure distribution because when separation appears, the aerofoil behaves a little more

like a bluff body. To handle flows over bluff bodies, Parkinson [10] implanted sources at the surface of bodies in potential-flow to simulate their wake. The pressure distribution obtained outside the separated region was in very good agreement with experimental results. Parkinson [11] extended his theory to the simulation of flow past aerofoils with a spoiler or a splitter plate. In both these problems, the position of separation is prescribed and is not predicted. In the simulation of flow past aerofoils, sources are also used to simulate the separated wake. The potential describing the flow about the aerofoil is dependent on five variables and five closure conditions are used to find appropriate values for these variables. One of these conditions requires the experimental base pressure, which is then an important input to the model to predict the right lift and pressure distribution around the aerofoil. Nevertheless, the results obtained by Parkinson are good and they show that it is possible to obtain a good simulation of the pressure distribution around an aerofoil with separated flow by implanting sources in the potential flow.

Numerical methods that can make use of a pressure distribution that can be modified by the presence of sources, are methods based on inviscid-viscous calculations. In this approach, potential flow theory is used to provide the pressure distribution for boundary-layer calculations. Based on these results, the potential flow is modified for the boundary-layer displacement thickness until after further iterations, convergence is satisfied. For viscous flow over streamlined surfaces, such iterative methods have been used for many years and have proved to be sufficiently accurate for the useful prediction of lift, drag and other aerodynamics parameters. But in the case of separated flows, two extra complications arise. The pressure distribution around an aerofoil is influenced in an increasingly uncertain manner by the presence of a separated region and the exact position of separation is unknown *a priori*.

The pressure distribution obtained by simulating the separated region

with sources, can be used in a boundary-layer calculation to determine the evolution of the skin friction coefficient on the extrados of the aerofoil. The smallness of this coefficient gives an indication of where the separation point can be found. Hence the use of a boundary-layer calculation in the theoretical model provides the basis of a closure condition that can regulate the point of separation.

Flow separation is a fully elliptical problem, *i.e.* the separated region modifies the whole flow behaviour around the aerofoil, which in turn influences where the flow separates and so on. So a time-averaged steadied separation position converges to a point that stabilizes the flow configuration. An iterative procedure to find the position of separation seems, in that case, a very appropriate approach. Hence with sources to simulate the separated region in a potential flow and an adequate set of closure conditions to ensure a realistic flow about the aerofoil, an iterative scheme may be developed to find the position and the strength of the sources.

Beside the modification of the pressure distribution, the presence of the sources near the trailing-edge has other effects on the flow field. Obviously over the sources, the streamlines of the main flow are pushed away from the surface similarly to streamlines over a separated region. The circulation needed to satisfy the Kutta condition is reduced in the presence of the sources near the trailing-edge, which results in a reduction of lift. In a real flow lift is reduced when separation occurs. Finally, the aerofoil needs to be set at an higher angle of attack in order to have the stagnation streamline attaching at the position it did before the introduction of the source. In the case of a circular-arc, when sources are present near the trailing-edge, the design incidence is not zero any more. A real aerofoil with separation at design incidence has a design incidence greater than what an inviscid flow predicts. So sources used in a potential flow exhibit the general effects of a separated flow.

Hence the aim of the present research is to develop a potential flow and boundary-layer model that predicts the lift coefficient, the location of separation, the pressure within the separated region, the design incidence and the drag coefficient of a circular-arc aerofoil simply by providing its camber ratio and Reynolds number. The model is independent of any empirical relations although some of the closure conditions require further substantiation. Results are measured on an experimental model to evaluate the accuracy of the numerical predictions.

The circular-arc has a major advantage, it is a special case of the Joukowski transformation and thus provides an analytical solution for the numerical model. But the aerofoil has a sharp leading-edge and, as was mentioned above, separation bubbles will appear at the leading-edge of the experimental model, either on the pressure or on the suction side of the aerofoil depending on the angle of attack. After reattachment, the growth of a boundary-layer is different from the growth of a regular boundary-layer (Bradshaw [1]). Only at design incidence will the fluid smoothly flow around the leading-edge. It was decided to isolate the effect of the trailing-edge separation by studying the circular-arc aerofoil at design incidence. But probably the most important reason is to ensure a regular growth of boundary-layer to help the boundary-layer calculations to give good results. It was also decided to simulate a turbulent flow separation on the aerofoils.

Chapter 2

Theory

In this chapter, the theoretical model is described in detail. The mathematical formulation of the potential flow is developed in its initial approach with a set of proposed hypotheses to close the problem. These hypotheses are therefore closure conditions. The modifications needed to make the model converge to a realistic solution are discussed and the final version of the theoretical model is described.

A brief overview of the initial numerical model is given here. The aim of the theoretical model is to obtain, as a final result of the simulation, a potential flow that simulates closely a real flow around an aerofoil with separation. The potential flow uses sources implanted on the surface of the aerofoil near the trailing-edge to simulate a separated wake and its effect on the pressure distribution around the aerofoil. The initial model used a uniform distribution of constant sources on the aerofoil, and this configuration gives a potential flow that is influenced by six variables. Non-dimensionalizing the complex velocity equation with the free-stream velocity U, it is found that the pressure distribution depends only on five variables. Hence, in order to find a specific value for each of these variables, five closure conditions are needed. From initial guess

values, the distribution and strength of the sources are modified iteratively until the five conditions are satisfied. These conditions are described in section 2.2. Once the solution converges, the following are predicted:

- pressure distribution (C_p) and base pressure (C_{pb})

- separation position

- design incidence (α_d)

- lift coefficient (C_L)

- drag coefficient (C_D)

2.1   Initial Potential Flow

In potential flow theory, flow around a circular arc aerofoil is obtain from a special case of Joukowski's transformation of the flow around a circular cylinder. The flow around the circular cylinder is obtained by putting a doublet directly oriented in a uniform stream. One streamline of this arrangement is perfectly circular and is taken as the boundary of the cylinder. The field around the cylinder can be mapped onto a field around a circular arc. The transformation from one plane to the other is given by the following relation

$$\varsigma = (z + ic) + \frac{a^2}{(z + ic)} \tag{2.1}$$

Figure 2.1 gives a schematic representation of the mapping. The transformation circle has a radius a, smaller than the radius of the cylinder b. As shown on figure 2.1, the transformation circle is shifted down until the edge of the cylinder intersects with the maximum thickness of the circle. These two points of the transformation are singular (or not conformal). The camber of the arc is determined by c, the offset distance between the two centres.

8

To add circulation in the flow a vortex of strength Γ is placed at the centre of the cylinder. The superposition of this vortex with the other elements of the flow, modifies the streamlines around the cylinder and the two surface stagnation points are moved toward the imaginary axis. When the right amount of circulation is added, it is possible to bring the rear stagnation point to the singular point that transforms into the trailing-edge. It happens that when the stagnation point is brought there, the velocity found at the trailing-edge of the aerofoil is finite. The details of this transformation of a stagnation into a point of finite velocity are given in section 2.2.1. After setting the basis for a uniform flow around an aerofoil, a uniform distribution of sources may be placed on a section of its surface.

In order to put a source in the flow field without distorting the cylinder surface, a matching source must be placed at the corresponding inverse point inside the cylinder. To absorb the spilling of the matching source, a sink of equal strength must also be placed inside the cylinder in order to keep the cylinder closed. The same reasoning applies for the sink, hence a matching sink of equal strength must be located at the inverse point of the first one, outside of the cylinder. Noticing that the inverse point of the centre of the cylinder is at infinity and knowing that a sink placed at infinity does not affect the flow close to the origin, it becomes clear that the draining sink inside the cylinder must be located at the centre. These considerations are only applications of the circle theorem, as described by Milne-Thomson [7].

The strength of point sources, sinks or vortices is not affected by mapping, *i.e.* a point source will be geometrically mapped onto an other part of the space but will remain of the same strength. Distributions of sources, sinks and vortices are affected by mapping because they have the units of strength/length and mapping distorts the space, thus affecting the lengths. Hence the distribution of sources on the cylinder will not be the final distribution on the aerofoil.

9

In order to get the right distribution of sources in the transformed plane, the following requirement must be met

$$\sigma \left|dz\right|_{z=be^{i\theta}} = m \left|d\varsigma\right|_{z=be^{i\theta}} \qquad (2.2)$$

where σ is the strength distribution of continuous sources on the cylinder and m is the corresponding constant distribution on the aerofoil (see figure 2.1). This leads to

$$\sigma = m \frac{\left|d\varsigma\right|_{z=be^{i\theta}}}{\left|dz\right|_{z=be^{i\theta}}} = m \left|\frac{d\varsigma}{dz}\right|_{z=be^{i\theta}} \qquad (2.3)$$

which can be evaluated using eq. 2.1 to give the final result

$$\sigma = m \left|\frac{2b(c + b\sin\theta)}{b^2 + 2bc\sin\theta + c^2}\right| \qquad (2.4)$$

A short analysis of the denominator of this function shows that

$$
\begin{aligned}
b^2 + 2bc\sin\theta + c^2 &= (b+c)^2 - 2bc(1 - \sin\theta) \\
&> (b+c)^2 - 4bc \\
&> (b-c)^2 \\
&> 0
\end{aligned}
$$

Hence if the denominator of eq. 2.4 is always positive, then this function is periodic with zeroes satisfying the equation

$$
\begin{aligned}
c + b\sin\theta &= 0 \\
\sin\theta &= -\frac{c}{b}
\end{aligned}
$$

corresponding to $\theta = -\tau$ and $\theta = \pi + \tau$, which are the singular points of the transformation.

The complex potential for this given distribution of sources and for a variable aerofoil incidence α is given by

$$F(z_1) = U\left(z_1 + \frac{b^2}{z_1}\right) + i\frac{\Gamma}{2\pi}\ln z_1 + \int_{\delta_1}^{\delta_2} \frac{\sigma}{2\pi} b\left[\ln(z_1 - be^{i(\theta-\alpha)}) - \frac{1}{2}\ln z_1\right] d\theta \qquad (2.5)$$

where $z_1 = ze^{-i\alpha}$. It follows that

$$\frac{d}{dz} = \frac{d}{dz_1}\frac{dz_1}{dz} = e^{-i\alpha}\frac{d}{dz_1} \qquad (2.6)$$

and hence differentiating the complex potential to get the velocity potential gives

$$W(z) = e^{-i\alpha}\frac{d\,F(z_1)}{dz_1}\bigg|_{z_1=ze^{-i\alpha}} \qquad (2.7)$$

$$W(z) = Ue^{-i\alpha}\left(1 - \frac{b^2}{z_1^2}\right) + i\frac{\Gamma}{2\pi}\frac{e^{-i\alpha}}{z_1} + \int_{\delta_1}^{\delta_2}\sigma\frac{b}{2\pi}\left(\frac{e^{-i\alpha}}{z_1 - be^{i(\theta-\alpha)}} - \frac{e^{-i\alpha}}{2z_1}\right)d\theta\bigg|_{z_1=ze^{-i\alpha}}$$
$$(2.8)$$

$$W(z) = Ue^{-i\alpha}\left[1 - \left(\frac{b}{ze^{-i\alpha}}\right)^2\right] + i\frac{\Gamma}{2\pi}\frac{1}{z} + \int_{\delta_1}^{\delta_2}\sigma\frac{b}{2\pi}\left(\frac{1}{z - be^{i\theta}} - \frac{1}{2z}\right)d\theta \qquad (2.9)$$

Because the sources are put on the upper surface of the aerofoil, $\delta_1 > -\tau$ and $\delta_2 < \pi + \tau$ thus σ will always be positive and the absolute value sign can be ignored. The velocity potential is then found to be

$$W(z) = Ue^{-i\alpha}\left[1 - \left(\frac{b}{ze^{-i\alpha}}\right)^2\right] + i\frac{\Gamma}{2\pi}\frac{1}{z} + \int_{\delta_1}^{\delta_2}\frac{mb^2(c + b\sin\theta)}{\pi(b^2 + 2bc\sin\theta + c^2)}\left(\frac{1}{z - be^{i\theta}} - \frac{1}{2z}\right)d\theta$$
$$(2.10)$$

The integral part of this equation is solved analytically to give the velocity potential in the final form

$$u - iv = \frac{dF}{dz} \qquad (2.11)$$

$$\frac{1}{U}\frac{d\,F(z)}{dz} = e^{-i\alpha}\left[1 - \left(\frac{b}{ze^{-i\alpha}}\right)^2\right] + \frac{i}{2\pi}\frac{\Gamma}{U}\frac{1}{z} +$$

$$\frac{mb^2}{4\pi Uz(zc + ic^2)(zc + ib^2)}\left\{z(c^2 - b^2)\ln\left(\frac{b^2 + 2b\sin\delta_2 + c^2}{b^2 + 2b\sin\delta_1 + c^2}\right) + \right.$$

$$\left[4c^2z - 2ic(z^2 - b^2)\right]\ln\left(\frac{z - be^{i\delta_1}}{z - be^{i\delta_2}}\right) + i(z^2 + b^2)\ln\left[\frac{(be^{i\delta_2} + ic)(b - ice^{i\delta_1})}{(be^{i\delta_1} + ic)(b - ice^{i\delta_2})}\right] +$$

$$\left. c(z^2 - b^2 + 2icz)(\delta_2 - \delta_1)\right\} \qquad (2.12)$$

11

This equation gives the velocity, in non-dimensional form, at any point z around the circular cylinder. To obtain the corresponding velocity on the circular-arc, a simple chain rule is used, giving

$$
\begin{aligned}
(u - iv)_\varsigma &= \frac{dF}{d\varsigma} \\
&= \frac{dF}{dz}\frac{dz}{d\varsigma} \\
&= \frac{dF}{dz} \; \frac{1}{1 - \left(\frac{a}{z+ic}\right)^2}
\end{aligned}
\tag{2.13}
$$

From this velocity equation, the pressure coefficient can be found using the relation

$$
C_p = 1 - \left(\frac{u^2 + v^2}{U^2}\right)
\tag{2.14}
$$

The geometry of the aerofoil fixes the values of a, b and c. In non-dimensional form, the remaining variables that can modify the flow are: $\alpha, \frac{\Gamma}{U}, \frac{m}{U}, \delta_1$ and δ_2. Five closure conditions are used to make the potential flow exhibit realistic characteristics found on real separated aerofoils. These conditions ensure a unique value for each of these variables.

2.2 The closure conditions

2.2.1 Kutta condition

In any real flow about an aerofoil, the pressure at the trailing-edge is never excessively low, showing that there is not an extreme curvature of the streamlines in this region. Experimental observations demonstrate that a time-averaged streamline leaves from the trailing-edge. This condition is common to any aerofoil; it is then essential that the potential flow also exhibits this characteristic. It is possible to force a streamline to leave the aerofoil at the trailing-edge, by

12

imposing the appropriate circulation on the circular cylinder, so that the point that will be mapped onto the trailing-edge is a stagnation point. This ensures that the fluid flows smoothly about the trailing-edge and that there will not be any sharp curvature of the streamlines in that neighbourhood, thereby guaranteeing a finite pressure there. The point from which the streamline leaves the cylinder is a stagnation point or a point of zero velocity. Hence, this condition is stated in the circle plane as follows

$$\left. \frac{dF(z)}{dz} \right|_{z=be^{-i\tau}} = 0 \qquad (2.15)$$

where $z = be^{-i\tau}$ is the point mapped to the trailing-edge of the circular-arc. The stagnation point is brought to a point where the transformation is not conformal. Evaluating the velocity in the circular-arc plane there gives an indeterminate ratio of $\frac{0}{0}$. L'Hopital's rule gets over this indeterminate form and gives a finite velocity at the trailing-edge. The Kutta condition is one of the most important and basic condition in this model. Figure 2.2 shows the streamline configuration around the trailing-edge when the condition is satisfied.

2.2.2   Design incidence

At a precise angle of attack, a streamline stagnates exactly on the leading-edge of an aerofoil. This angle of attack is called the design incidence. In the present case, it avoids a leading-edge separation bubble on the extrados which would make calculation of the boundary-layer difficult [1]. In order to get a streamline attaching at the leading-edge of the aerofoil, a stagnation point must be located, in the circle plane, on the point that will be mapped to the leading-edge. This point is at the intersection of the circular cylinder and the circle of transformation, at $\theta = \tau + \pi$ (see figure 2.1). This condition is in fact a Kutta condition applied to the leading-edge. It is stated in the circular cylinder

plane as

$$\frac{dF(z)}{dz}\bigg|_{z=be^{i(\tau+\pi)}} = 0 \qquad (2.16)$$

where $z = be^{i(\tau+\pi)}$ is the point mapped to the leading-edge of the circular-arc. The streamlines around the leading-edge are represented graphically on figure 2.3, for an aerofoil at design incidence.

2.2.3   Base pressure hypothesis

When sources are put on the surface of an aerofoil, a stagnation point appears on the aerofoil, in front of the sources. A streamline leaves the aerofoil from that point. From the potential flow, a complete pressure distribution around the aerofoil is obtained. The pressure on the extrados of the aerofoil is used in a turbulent boundary-layer development calculation to determined a point of separation. This boundary-layer method is described in section 2.3. The boundary-layer calculations uses the part of the pressure distribution in front of the sources. This distribution is very similar to the pressure distribution found ahead of separation on a real aerofoil. Using this distribution, the boundary-layer calculation provides a realistic point of separation. Separation in this model occurs then before the stagnation point mentioned above. Considerations about the separation point, the stagnation point and the separating streamline are discussed in sections 4.1.1 and 4.1.2.

In a real flow, because of the high degree of turbulence that is encountered in the separated wake of an aerofoil and mostly because of the mixing associated with this turbulence, the time-averaged pressure is nearly constant throughout this wake. The value of this pressure is known as the base pressure for flow over bluff bodies. Figure 4.1 shows a measured pressure distribution around a circular-arc aerofoil with separation, where the region of constant pressure (base pressure) is clearly visible. This is characteristic of aerofoils with sep-

14

arated wakes. It is desirable that the potential flow presents the essence of this observation. The wake being situated between the trailing-edge and the separation point, it implies that these two points are practically at the same pressure. To transpose this observation in the model, a condition requires that the pressure at which the flow separates, be the same as the one found at the trailing-edge. This condition can be stated numerically as follow

$$C_p|_{sep} = C_p|_{t\,e} \tag{2.17}$$

Thwaites [17] proves the validity of a similar condition for viscous flow about bluff bodies.

2.2.4 Lift hypothesis

Experimentally, on a real aerofoil, the lift can be determined in several ways. One possible approach, is to consider the circulation, Γ, in a large circuit around the aerofoil [17] and use the Kutta-Joukowski relation

$$L = \rho U \Gamma \quad or \quad C_L = \frac{2\Gamma}{UC} \tag{2.18}$$

Another one, is to sum up the pressure distribution and the skin friction when resolved in the proper direction. These two different ways of measuring the lift, are expected to give the same result.

It is also possible to obtain the lift in potential flow in several ways. In the model, the total amount of circulation around the aerofoil is equal to the strength of the vortex situated in the middle of the circular cylinder. The strength of this vortex is not modified by the conformal transformation. Here also, the total lift is given by eq. 2.18.

Integrating the pressure distribution around the aerofoil, to find the lift, would automatically give the same result found as using the circulation. Nothing new would be brought into the problem. But in the model, the sources are

15

used to simulate the pressure distribution found around a real aerofoil, <u>outside</u> the wake. The variation of pressure close to the sources within the wake is unrealistic compared to what is observed experimentally. To get a realistic pressure distribution over the entire aerofoil, the pressure from the point of separation to the trailing-edge can be empirically modified and put equal to the pressure found at the separation point. This modified pressure distribution can be compared with experimental data all around the aerofoil. The lift on the aerofoil can be found by integration of this pressure distribution.

$$C_l = \oint C_{pm} dx'$$ (2.19)

where C_{pm} is the <u>modified</u> pressure distribution and x' is the coordinate in the direction of the free-stream flow. As the source strength and their position are modified to simulate a pressure distribution closer to the experimental one, eq. 2.19 computes a lift coefficient closer to the result sought by the simulation. It is therefore suggested that in order to get a consistent pressure distribution, the two different ways of computing the lift — *i.e.* eq. 2.18 and eq. 2.19 — should give the same result. In other words, satisfying the condition

$$\oint C_{pm} dx' = \frac{2\Gamma}{UC}$$ (2.20)

gives to the potential flow a characteristic belonging to any flow around a real aerofoil with a separated wake.

2.2.5   Drag hypothesis

In real flows about aerofoils, the magnitude of drag can be deduced from the velocity distribution in the wake. For two-dimensional flow, the total drag per unit depth on a body is given by the expression

$$D = \rho \int_{-\infty}^{\infty} u(U - u) dy$$ (2.21)

$$= \rho U^2 \theta$$ (2.22)

16

where U is the free-stream velocity, $u(y)$ is the velocity distribution in the wake and θ is the momentum thickness. Once the flow has left the aerofoil, θ only changes due to the downstream variations of pressure. Far from the aerofoil, where the pressure settles, for any velocity traverse the momentum thickness is constant. Hence the drag can be measured from the velocity profile in the wake at any distance sufficiently faraway from the aerofoil. In that case, the difference between the velocity profile in the wake and the free-stream velocity is small. As a consequence, the displacement thickness, measured in a wake far downstream of an aerofoil, is approximately equal to the momentum thickness [17].

$$\delta^*_{real} \cong \theta_{real} \tag{2.23}$$

In the potential flow, the sources are injecting fluid that pushes the streamlines apart. Far from the aerofoil, the streamlines are separated by a constant distance that can be associated with the displacement thickness. The linkage between the potential flow and the real flow is done here by assuming that

$$\delta^*_{pot} = \delta^*_{real} \tag{2.24}$$

The source distribution on the aerofoil $m\,ds$ is such that

$$\int_S m\,ds = U\delta^* \tag{2.25}$$

where S is the length over which the sources are distributed and m is the strength of the sources per unit length. Using eq. 2.22 and eq. 2.23, the drag is related to the sources by

$$D = \rho \int_S m\,ds \quad or \quad C_d = \frac{2m\Delta}{UC} \tag{2.26}$$

where Δ is the total length of sources and C is the aerofoil chord. G.I. Taylor [16] used the concept to simulate the drag of very porous plates and Prandtl [13] used it to calculate the wake interference in closed wind tunnel, a method that is still in use today.

17

In the previous section, the <u>modified</u> pressure distribution around the aerofoil is integrated to find the lift. Similarly, the pressure drag on the aerofoil can also be found from the modified pressure distribution. In that case

$$D = \oint p_m dy' \quad or \quad C_D = \oint C_{pm} dy' \tag{2.27}$$

where y' is the coordinate normal to the free-stream direction.

If the skin friction drag is neglected and the total drag is approximated by the pressure drag, a fifth condition would be to equate the drags computed from these two independent ways. Hence

$$\oint C_{pm} dy' = \frac{2m\Delta}{UC} \tag{2.28}$$

is the last condition.

This last hypothesis is really the weakest of the five conditions described above. Some of the assumptions that are defendable in the case of flows over aerofoils with no separation, become less defendable for flows with large regions of trailing-edge separation. Eq. 2.23 and eq. 2.24 are stating the two assumptions that are most likely to be too crude to help the numerical method to give accurate predictions. The condition is used anyway to close the initial model.

These are the initial five conditions.

2.3   Boundary layer development method

The simulated flow over the aerofoil is assumed to be turbulent. The velocity distribution is given by the potential flow part of the calculation and fed in a boundary-layer development method to predict the evolution of the skin friction coefficient on the upper surface of the aerofoil. When the skin friction coefficient gets very close to zero, the flow is considered to separate. For this part of

18

the calculation, several methods were available. The criteria of selection were mainly accuracy and simplicity.

An integral method developed by Head and Patel [3] was found to fulfil those requirements and was used. This method is based on the entrainment principle that makes the assumption that the rate at which free-stream fluid is incorporated into the boundary layer is determined by the velocity defect in the outer part of the layer, and was first proposed by M. R. Head [4]. The method used here is an improvement on his original entrainment method. The entrainment was modified to ensure agreement with measured equilibrium layers. For layers proceeding to separation the entrainment is reduced, and for layers where H is decreasing it is increased. This method gives very good predictions when compared with experimental results of different types of flows (see [3]) and the coding is straightforward. The boundary layer development is assumed to take place on a flat surface, *i.e.* the effect of curvature is neglected.

2.3.1   Starting conditions for the B.L. calculations

At first it was intended to use a laminar boundary-layer calculation coupled with a transition theory to find the starting position of the turbulent boundary-layer calculation and the initial values for the shape factor and the momentum thickness. But calculations using initial conditions found from results of flow over flat plates, indicated that the turbulent boundary-layer calculations are not very sensitive to these initial conditions. The starting position of the calculation (*i.e.* transition position) can be located ahead of $0.3C$ on the aerofoil without changing the predicted position of separation. A variation of 20% in the initial shape factor or a variation of 25% in the initial momentum thickness did not influence significantly the prediction of separation either. Hence using some approximations, initial values were chosen. The transition position was found assuming

19

the aerofoil to be a flat plate, using a laminar boundary-layer development and a transition criteria based on the momentum thickness. The initial shape factor and momentum thickness used are typical values found on a flat plate after transition $i.e.$ $R_\theta = 800$ and $H = 1.4$ (Young [21]). Because these values gave good results for the prediction of separation, it was decided not to incorporate a laminar boundary-layer calculation coupled to a more sophisticated transition theory thereby keeping the actual model as simple as possible.

2.4　The iterative scheme

An iterative scheme was developed to obtain a converged solution where all the five closure conditions are satisfied. The Kutta condition was used to explicitly find the circulation Γ as a function of the other variables.

$$\frac{\Gamma}{U} = 4\pi b \sin(\tau + \alpha) + \frac{mb\{\ldots\}_K}{2Uc(b^2 - 2b\sin\tau + c^2)} \tag{2.29}$$

where

$$\{\ldots\}_K = \left\{ b(c^2 - b^2) \ln\left(\frac{b^2 + 2b\sin\delta_2 + c^2}{b^2 + 2b\sin\delta_1 + c^2}\right) + \right.$$
$$2bc(c - b\sin\tau)\left[2\ln\left(\frac{1 - e^{i(\delta_1+\tau)}}{1 - e^{i(\delta_2+\tau)}}\right) + i(\delta_2 - \delta_1)\right] +$$
$$\left. 2ib^2c\cos\tau\ln\left[\frac{(be^{i\delta_2} + ic)(b - ice^{i\delta_1})}{(be^{i\delta_1} + ic)(b - ice^{i\delta_2})}\right]\right\}$$

Equation 2.29 was then used to replace Γ in the design incidence condition. From this new equation, and after some simplifications, the following relation was derived.

$$-4i\cos\tau\sin\alpha + \frac{m}{U}\frac{\{\ldots\}_K + \{\ldots\}_D}{4i\pi c(b^2 - 2\sin\tau + c^2)} = 0 \tag{2.30}$$

where

$$\{\ldots\}_D = \left\{ -b(c^2 - b^2)\ln\left(\frac{b^2 + 2b\sin\delta_2 + c^2}{b^2 + 2b\sin\delta_1 + c^2}\right) - \right.$$

20

$$2bc\left(c - b\sin\tau\right)\left[2\ln\left(\frac{1 + e^{i(\delta_1 - \tau)}}{1 + e^{i(\delta_2 - \tau)}}\right) + i(\delta_2 - \delta_1)\right] +$$

$$2ib^2 c\cos\tau\ln\left[\frac{\left(be^{i\delta_2} + ic\right)\left(b - ice^{i\delta_1}\right)}{\left(be^{i\delta_1} + ic\right)\left(b - ice^{i\delta_2}\right)}\right]\Bigg\}$$

From initial guess values of the source strength m and of the distribution δ_1 and δ_2, α is found from eq. 2.30, then Γ is found explicitly using eq. 2.29. The constant base pressure condition is used to modify the source strength (m), the lift condition to modify the position where the distribution of the sources begins (δ_1) and the drag condition to modify the position where the distribution stops (δ_2). The computation of α and Γ is done after a modification to any one of the other three variables. The last three conditions are used alternatively until the convergence of the five variables.

2.5   Preliminary results

When the iterative scheme described above was implemented and tested, convergence was achieved but all the predicted values of lift, drag, *etc.* were very different from experimental values. As mentioned in section 2.2.5, the hypothesis that seemed to be the weakest was the drag condition. Therefore it was abandoned and the strength of the sources was chosen. A series of tests was done for a whole range of strengths and the best agreement with the measurements (to be described later) were obtained for a very large injection velocity and practically no distribution length.

This result suggested that the distribution of sources might be replaced by a point source. With the drag condition abandoned and the use of a point source instead of a distribution, the numerical model adopts more Parkinson's approach for the simulation of a separated wake than the idea of the simulation of the entrainment of the main flow in the wake. Parkinson used two point

21

sources to simulate a wake and the position of separation was physically fixed. The present model is using a single point source and the position of separation is calculated, which is believed to be an improvement.

If a single point source is used, the potential flow is now dependent on four variables since a single variable is needed to position of a point source instead of two variables to fix a continuous distribution of sources. With four variables to shape the flow and the first four closure conditions, a unique value can be found for each variable. Because the four hypotheses have a sounder experimental basis, the calculated flow, at convergence, is realistic and gives good results. The final version of the potential flow part of the theoretical model is described below.

2.6 Final potential flow

The potential is basically the same, the integral part is replaced by the potential of a point source on the cylinder and a point sink of half its strength at the centre. The complex potential is then

$$F(z_1) = U\left(z_1 + \frac{b^2}{z_1}\right) + i\frac{\Gamma}{2\pi}\ln z_1 + \frac{M}{2\pi}\left(\ln(z_1 - be^{i(\delta-\alpha)}) - \frac{1}{2}\ln z_1\right) \quad (2.31)$$

$$z_1 = ze^{-i\alpha} \quad (2.32)$$

Similarly the complex velocity is obtained by the differentiation of the potential.

$$\frac{dF(z)}{dz} = Ue^{-i\alpha}\left[1 - \left(\frac{b}{ze^{-i\alpha}}\right)^2\right] + i\frac{\Gamma}{2\pi}\frac{1}{z} + \frac{M}{2\pi}\left(\frac{1}{z - be^{i\delta}} - \frac{1}{2z}\right) \quad (2.33)$$

Figure 2.4 shows a schematic representation of the final mathematical model which was used.

22

2.7 Final iterative scheme

The final iterative scheme is very similar to the initial one. Γ is still expressed explicitly using the Kutta condition. The expression is now

$$\frac{\Gamma}{U} = 4\pi b \sin(\tau + \alpha) + \frac{M}{U} i \left(\frac{1}{1 - e^{i(\delta + \tau)}} - \frac{1}{2} \right) \qquad (2.34)$$

Using this result, α is now found in this relation

$$8\pi b \cos \tau \sin \alpha + \frac{M}{U} i \left(\frac{1}{1 - e^{i(\delta + \tau)}} - \frac{1}{1 + e^{i(\delta - \tau)}} \right) = 0 \qquad (2.35)$$

α is a function of δ and M and can be found easily. Then replacing α in eq 2.34 , Γ is found. Much simpler mathematical formulation is associated with the use of a point source.

The scheme starts again from initial guessed values for the source strength and its position. The constant pressure condition is used to modify the source strength (M), and the lift condition is used to modify its position (δ). The iterations and the calculations are done in the same sequence. After any modification to M or δ, α and Γ are recomputed before any new modification of the strength or position of the source. The iteration scheme goes on until the four conditions are satisfied.
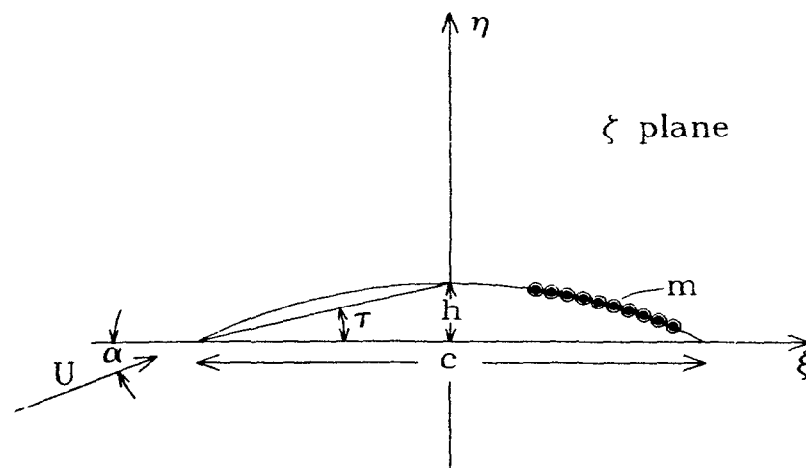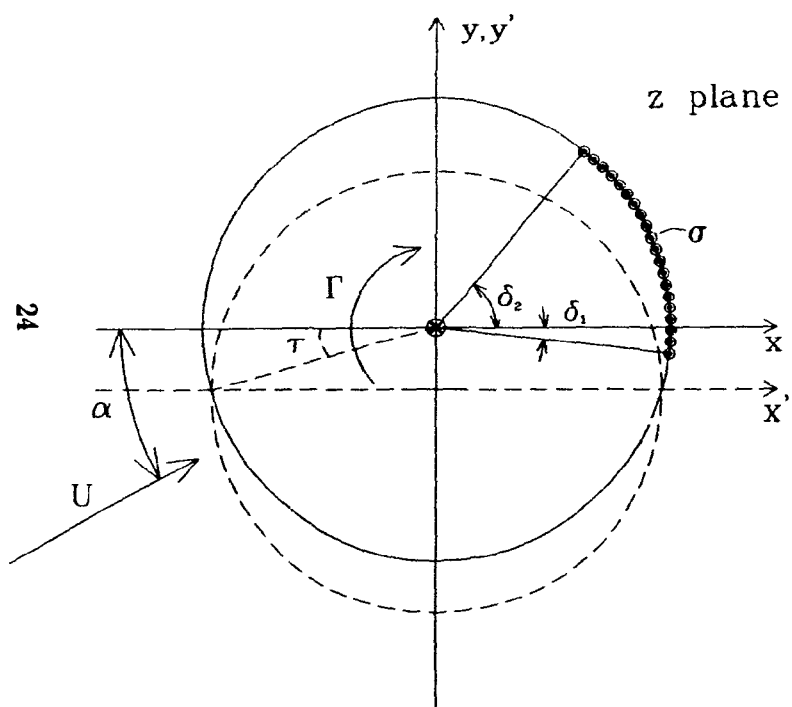
Figure 2.1: Transformation of the circular cylinder into a circular-arc aerofoil

Figure 2.2: Streamlines around the trailing edge satisfying the Kutta condition

Figure 2.3: Streamlines around the leading edge of the aerofoil at design incidence
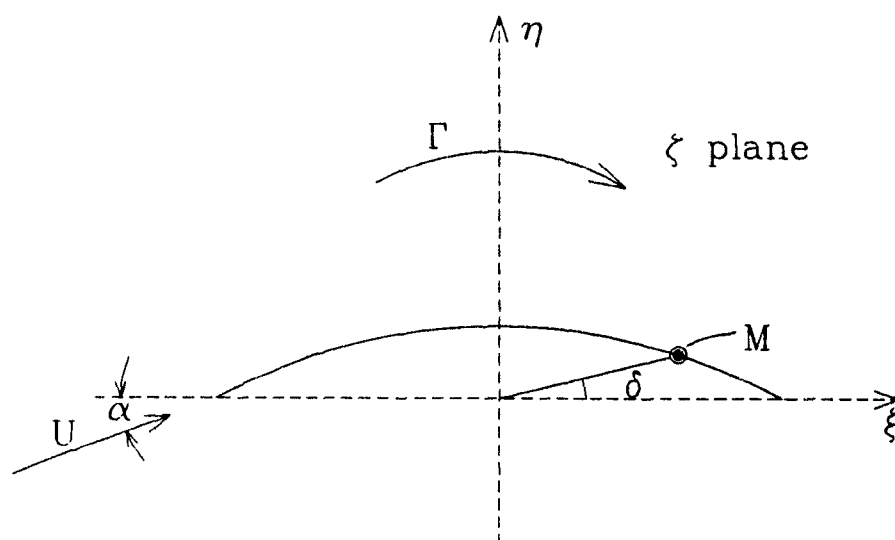
Figure 2.4: Representation of the final mathematical model

Chapter 3

Experiment

3.1 Apparatus

3.1.1 Experimental set-up

For the experiments, the different apparatus and instruments, described below, have been arranged and interconnected to measure the desired characteristics of the aerofoil. Figure 3.1 gives a schematic representation of the experimental set-up. The linkage between the different elements of the set-up can be divided in two groups; one controlling the wind tunnel and one acquiring and processing the data of the aerofoil.

The control of the wind tunnel is completely independent and was only used to set the air flow at the desired speed. The measuring system, was controlled by the data acquisition system programmed into the computer. In this system, the experimental model was attached to a balance, decomposing the resultant aerodynamic force in two perpendicular components. These two components were sent to the computer as inputs for the data acquisition system.

The pressure taps inserted in the aerofoil were connected to the pressure selector. Pressure lines carrying the reference pressure of the wind tunnel, used to measure the wind speed, were also connected to the scanivalve. This pressure selector sent one pressure to the pressure transducer, which sent a third input to the acquisition system. The computer read the input signals and controls the pressure selector. A photograph of the set-up is shown in figure 3.2.

3.1.2 Wind tunnel

The McGill 3ft.×2ft. wind tunnel, shown in figure 3.3 [20], is an open return wind tunnel with a closed working section 914 mm wide by 610 mm high in cross-section, and approximately 2.04 m in length. The intake is two-dimensional with parallel vertical walls, and upper and lower walls converging at an angle of 90°. The converging walls merge into the working section through a curved section whose shape is based on the free streamline solution for flow emerging from two converging plates. This prevents separation and establishes a rather uniform flow in the working section. The intake is fitted with a 14 mesh, 0.56 mm diameter curved gauze followed by a 6.4 mm by 25.4 mm deep curved honeycomb to straighten the flow and reduce turbulence.

Behind the working section is a rectangular diffuser followed by a transition section from rectangular to circular cross-section. At the end of this section is a five-bladed Buffalo Forge 54s Type B Vane axial fan driven by a 40 hp d.c. motor to speeds up to 1150 rpm. A Ward-Leonard control system, consisting of a 550 V three phase a.c. motor driving a d.c. generator, supplies power to the d.c. fan motor. The fan speed is controlled by varying the current in the field windings of the generator. This system provides a smooth speed control in the working section from zero to nearly 50 m/s. The outlet of the fan is connected to a large filter box, for the purpose of reducing noise, filtering the

28

air, and reducing the swirl in the returning air flow.

Due to the longitudinal growth of the boundary layers on all four walls of the working section, a small favourable pressure gradient exist in the longitudinal direction. In the initial calibration of the wind tunnel in 1961 [20], the pressure gradient was found to be

$$\frac{1}{\frac{1}{2}\rho\overline{U}^2}\frac{d\overline{p}}{dx} = -0.028 m^{-1}$$

at x = 1.33 m and approximately constant in the longitudinal direction. In a recent investigation by Storm [15], this pressure gradient was found to be slightly lower, *i.e.* $-0.023 m^{-1}$ for a floor that was perhaps smoother.

The r.m.s. turbulence in the free-stream of the working section is approximately 0.4 percent of the free-stream velocity and does not vary appreciably with tunnel Reynolds number [20].

3.1.3 Circular arc aerofoils

In order to get clear experimental values for the separation location on the aerofoil, it was decided to chose a camber that would have a 25% of chord separation at design incidence. The choice of the camber of the aerofoil was based on experimental results obtained by Tse [18] on three small circular arc aerofoils of 5%, 10% and 15%. According to these results, the 10% cambered aerofoil would give the desired result at design incidence. Thus a large 10% cambered aerofoil was constructed, but after preliminary testing it became clear that no separation was appearing on the model at design incidence. It is believed that the difference between Tse's observations on a smaller model and the observations made on the larger model in the present work, is due to a different interpretation of the behaviour of the tufts used to show separation. The present interpretation of the tufts is believed to take more into account the true nature of a separated

29

flow (see section 3.1.4). So a series of tests was conducted in a smoke tunnel on five circular arc aerofoils having cambers of 5%, 7.5%, 10%, 15% and 20%. For angles of attack ranging from 0 to full stall the separation location was recorded and the design incidence was found. These results can be found on figure 3.4 from which, by interpolation, a 25% separation at design incidence is expected to occur over an 18% cambered aerofoil. These tests were done at low Reynolds number, so these results have to be taken as approximations of higher Reynolds number results. Because the influence of the Reynolds number on the position of separation is very difficult to quantify, the results obtained in the smoke tunnel were directly used to select the camber of the larger aerofoil.

Hence in addition to the 10% cambered aerofoil already mentioned, another one of 18% camber was built. These aerofoils were cut out from a sheet of brass, 3.2 mm ($\frac{1}{8}$ in) thick, and were cold rolled to the desired camber. Each aerofoil had a chord of 22.86 cm (9.0 in) and a span of 60.64 cm (23.875 in) and, they were welded to end plates of 34.93 cm (13.75 in) long by 9.53 cm (3.75 in) wide and 3.2 mm ($\frac{1}{8}$ in) thick. These end plates were drilled in two places to allow attachment to the balance. On each side of the aerofoil, 34 pressure taps were located along the chord approximately half an inch apart and half an inch below mid-span. The pressure taps openings are photographed on figure 3.5. The pressure was collected at the surface of the aerofoil with small holes drilled through the aerofoil from one side to the other (fig. 3.6). These holes were connected to 1.6 mm ($\frac{1}{16}$ in) brass tubing inserted in the thickness of the aerofoil. When measurements were taken, the holes on one side of the aerofoil were blocked with thin adhesive tape to expose the openings of the pressure taps only to one side. A representation of the pressure taps openings is shown in figure 3.6. These tubes protruded from the bottom of the model, underneath the floor of the wind tunnel, and were connected to flexible tubing to bring the pressure out to the transducer. Figure 3.7 shows a schematic representation of an aerofoil with the inserted tubing and figure 3.8 is a photograph of the 18%

aerofoil with the flexible tubing.

3.1.4 Flow visualization

To visualize the behaviour of the flow over the extrados of the aerofoil, tertiary down feathers were glued to its surface. Those very fine tufts were individually selected for their dimensions and flexibility. They were attached to the surface by gluing their finest extremity with rubber cement and they were positioned vertically in order to have the same sensitivity to forward and back flow. A very small amount of glue, applied with the tip of a needle, was needed to attach the tufts to the surface of the aerofoil. The tufts were distributed all over the aerofoil on 13 rows of 17 tufts each. This configuration seemed to give a clear picture of the flow pattern without disturbing the flow too much.

A visualization technique was developed to give a better idea of the mean time behaviour of the tufts. In a turbulent flow, the tufts oscillate about a mean position. To keep track of the motion of the tufts, the surface of the airfoil is lightly powdered with white particles (talcum is used). The tufts act as sweepers and clean the areas over which they oscillate. Figure 3.9 shows the traces left by the tufts. The areas can be interpreted as follows:

- For laminar flow or slightly turbulent flow, the print of the tuft will be left on the surface of the airfoil. The print is small, in the direction of the flow and no sector has been cleaned.

- For turbulent fore flow, a whole sector has been cleaned and the middle of the circular edge of the sector indicates a mean time average of the direction of the flow.

- For turbulent back flow, the interpretation is the same as for turbulent fore flow. The only difference is in the orientation of the sector cleaned.

31

Because the back flow portion of the flow is very turbulent, the trace left in that region is larger than most of the traces left by the tufts in the fore flow. This can be seen at the right hand side of figure 3.9.

- In the vicinity of the separation point, the tufts will turn around in all directions, being influenced alternately by the forward and backward flow. In that case the traces left by the tufts will be full circles. For the range of Reynolds number for which the experiments were conducted, the separation point is an unsteady location moving forth and aft of a mean position. A steady separation leaves about 2 to 5 circles in a row from which the mean separation position is taken to be located in the middle of the line of circles. The mean is taken to be in the middle because it is believed to be the best estimate of the time-average position of separation.

A global picture of the traces left by the tufts on the aerofoil, after a run, is given in figure 3.10. A line shows where separation was interpreted to have occurred. This line joins all the middles of the section of circles, left by the separation line, on the rows of tufts. To the left of this white line, the sectors cleaned by the tufts indicate forward flow; to the right they indicate very turbulent back flow.

3.1.5 Force measurement

Balance

To measure the aerodynamic force, the aerofoil was attached to a balance made of two perpendicular load cells. The load cells are Model 462, manufactured by Transducer Inc. They use strain gages having a sensitivity of 2 mV/V with an excitation voltage of 10 V. The load cell measuring the X component can perceive a variation in force of $9.81 \times 10^{-3} N$ (0.001 Kg) and has a maximum

32

range of 223 N (50 lbs). The other one, measuring the Y component, can measure down to $1.96 \times 10^{-2} N$ (0.002 Kg) and has a maximum of 446 N (100 lbs). Each load cell is part of a whole system, composed of a programmable electronic unit that includes a power supply, a Wheatstone bridge and a voltmeter with an incorporated converter that gives the output reading in the desired units (N, Kg, lbf, lbs). The balance was built such that the two measured components of the force, $X \& Y$, are independent of each other. The programmable units are also equipped with a card that provides an output voltage, ranging from 0 V to 10 V, directly proportional to the measured force. These voltages were sent to a data acquisition system.

Lift and drag measurement

The balance is mounted in a sealed box attached to a large circular disc inserted in the wind tunnel floor. The bottom end of the aerofoil is attached to the balance and its chord is aligned with the most sensitive cell. To change the angle of attack of the aerofoil, the whole balance system is rotated. A scale fixed on the wind tunnel floor is used to measure the angle of attack. The drag and the lift are obtained from the recomposition of the two force components in the direction of the free-stream flow and its perpendicular direction. Figure 3.11 shows the measured force components and the direction of the lift and drag.

$$L = X \sin(\alpha + \epsilon) + Y \cos(\alpha + \epsilon) \tag{3.1}$$

$$D = -X \cos(\alpha + \epsilon) + Y \sin(\alpha + \epsilon) \tag{3.2}$$

The angle ϵ is the offset alignment between the orientation of the X component and the chord of the aerofoil. This offset angle is very important for the proper calculation of the drag. The angle ϵ is measured by applying a force perpendicular to the wind tunnel walls, on the aerofoil that was set exactly at zero angle of attack, i.e. the chord parallel to these walls. If there is an offset

33

angle between the balance and the aerofoil chord, there is a force measured by each component of the balance. The ratio of the two components is equal to the tangent of the offset angle ϵ. If there is no offset, the force applied is in line with one of the load cell of the balance and only one reading appears.

3.1.6 Pressure measurement

Pressure selector

In all, 34 tubes were used to collect the pressure from the aerofoil surface and 14 tubes were connected to the static reference pressure of the wind tunnel. Because only one electronic pressure transducer was available, all these pressures had to be selected sequentially. A Scanivalve of type 48D9-1135 was used for this purpose. The instrument was connected to the computer and controlled by the data acquisition program. The acquisition speed was set by the computer. When three successive readings of the pressure (aquired at a rate of 20 readings per seconds) were within 0.5% of each other, the computer sent a signal to the selector to switch the channel.

Pressure transducer

All pressure measurements were made using a Type 590 Barocel capacitive pressure sensor from Datametrics Inc. This transducer contains a flexible diaphragm within a capacitive cell. A pressure difference applied across the diaphragm causes it to flex, thereby changing the capacitance of the cell. The cell capacitance is accurately determined in an a.c. capacitance bridge and the corresponding output is rectified to a d.c. voltage ranging between -10 V and + 10 V. These limits are associated to the full scale of 10 inches of water for this instrument and the stated output accuracy is 0.1% of the full scale *i.e.* ±0.025

34

Pa. The Barocel was calibrated using the most sensitive pressure transducer available, an Askania water manometer accurate to $\pm 10 \mu m$ of water, or about ± 0.1 Pa. The calibration curve, shown in figure 3.12, is seen to be extremely linear over the entire range of the instrument; the calibration was found to be 241.645 Pa/V ($\pm 0.1\%$) and independent of the zero offset of the Barocel.

3.1.7 Data acquisition

The output of the pressure transducer and of the two force transducers were fed into a data acquisition system specially designed for aerofoil testing. The system was written using ASYST, a programming language designed for data acquisition, and it was installed on a PC/AT compatible computer. The A/D conversion and the control of the pressure scanner were done through a DAS-16F Metrabyte acquisition board. The board can accommodate up to eight differential signals and it uses a multiplexer to convert those signals sequentially. The frequency at which the acquisition is done, can be programmed.

The data acquisition system was constructed in three main parts. In the first part, uncorrected crude data like atmospheric pressure, air temperature, angle of attack, etc. were entered. The atmospheric pressure was then corrected and used with the air temperature to find density and viscosity of air. The rate at which the computer read the different instruments and the period over which the averages were calculated were also specified in the first part of the program.

The data acquisition was started in the second part; in sequence, the computer read the digitalized output of the pressure, and of the two force transducers. It then converted these numbers in dimensional quantities and sent them to the screen. The computer read the same pressure channel until three consecutive readings are within 0.5% of each other, then it sent a signal to the pressure selector to switch to the next channel and so on. In all of

35

the 48 pressure tubes connected to the selector, 34 were hooked to the aerofoil and 14 were connected to the reference static pressure of the wind tunnel. The wind tunnel speed was computed from this reference pressure and the calibration curve given in ref. [20]. This calibration curve was programmed into the computer so that the speed could be calculated directly and printed on the screen. The 14 tubes, bringing the wind tunnel reference pressure, were evenly scattered among the 48 tubes connected to the pressure selector, hence the wind tunnel speed was updated regularly. The aerofoil was scanned until the pressure distribution was found to be steady. Then the separation pattern was entered graphically on the screen with arrow pointers. All the accumulated data were then corrected for the different interferences of the wind tunnel and stored on files. The reader is referred to section 3.2 for more details about the treatment of the wind tunnel corrections.

The third part of the program is used to show or to print the collected data. Through different menus, the following plots can be accessed: C_L vs α, C_D vs α, from the balance and from the pressure distribution, C_p vs x for all α and separation location vs α.

3.2   Wind tunnel corrections

As mentioned above, in section 3.1.2, the experiments were conducted in a wind tunnel of rectangular cross-section. The size of the models tested justified the computation of corrections to take in account the effect of the restraining walls of the wind tunnel on the flow. These corrections have been studied over many years and they are now well known. The formulation used is the one found in Pope [12]. For general two-dimensional testing, four possible corrections are needed to attenuate the influence of the wind tunnel on the measurements. These are the buoyancy force correction, the solid and wake blockage corrections

and the streamline curvature correction due to lift.

The presence of thickening boundary-layers in the down stream direction on the walls of the tunnel, creates a pressure gradient in the test section. The model being tested, subject to this gradient, experience a buoyancy force acting downstream. If the pressure gradient is linear, this force is proportional to the volume of the aerofoil, as any buoyancy effect, and because the total volume of a circular-arc aerofoil is small, the buoyancy force is neglected.

Two blockage corrections are to be considered. The first one, the solid blockage correction, takes into account the reduction of cross-section area in the test section due to the presence of the model. As the flow passes by the model, a venturi effect is observed, increasing the velocity which results in a higher dynamic pressure that increases the lift and drag forces. But the solid blockage is dependent on the model thickness, the thickness distribution and on the model size compared to the cross-section of the test section. The thickness of the circular-arc is constant and very small compared to the width of the test section; hence the blockage correction is also neglected.

The other blockage effect to consider is the one due to the presence of a wake behind the aerofoil. Because the wake contains the viscous losses of the aerofoil, the velocity inside it is lower than the free-stream velocity. In the test section the mass flow is constant regardless of whether a wake is present or not. Since the mass flow in the wake is reduced, the one outside has to increase to maintain the total mass flow constant. The momentum lost in the wake is a measure of the drag of the aerofoil. It can also be related to the velocity increase in the free-stream flow due to the presence of the wake. The blockage correction, ϵ_{wb}, is estimated as a fraction of the uncorrected drag coefficient, C_{Du}, as follows:

$$\epsilon_{wb} = \frac{1}{2} \frac{chord}{tunnel\,width} C_{Du}. \tag{3.3}$$

37

The last important effect to take into account is the modification of the curvature of the streamlines due to the confinement of the flow. The walls of the wind tunnel straightened the streamlines and relative to these modified lines, the aerofoil appears to have more curvature. As a consequence, the aerofoil in a close wind tunnel as too much lift at a given angle of attack and even the angle of attack is larger as well. Replacing the aerofoil by a single vortex at its quarter-chord point and using a system of images, an effect on the lift and the angle of attack can be approximated. The quarter-chord point is chosen because it is the best estimate of the position of the centre of pressure.

The following expressions take in account all the wind tunnel corrections that were taken into account in the present thesis.

$$\alpha = \alpha_u + \frac{57.3\,\sigma}{2\pi}\,Clu \qquad (3.4)$$

$$C_l = C_{lu}\,[1 - 2\epsilon_{wb} - \sigma] \qquad (3.5)$$

$$C_d = Cdu\,[1 - 2\epsilon_{wb}] \qquad (3.6)$$

where

$$\sigma = \frac{\pi^2}{48}\,\frac{\text{chord}}{\text{tunnel width}} \qquad (3.7)$$

These corrections were implemented directly in the data acquisition system in order to obtain directly corrected results.

3.3 Uncertainty analysis

An uncertainty analysis is necessary to indicate the level of confidence people can have in experimental results presented. In this section, the uncertainty analysis performed for every computed result, is described. The analysis follows a standard method outlined by Moffat [6] in which the uncertainty on a

38

result (R), is determined as the root-sum-square of the individual uncertainties brought by each measurement entering in the composition of the result. In other words, for a given result (R), function of several variables X_i, each having its own uncertainty $\pm \delta X_i$, all given at the same odds, the uncertainty in R at the same odds is:

$$\delta R = \left[\sum_{i=1}^{n} \left(\frac{\partial R}{\partial X_i} \delta X_i \right)^2 \right]^{1/2} \tag{3.8}$$

In order to use this expression to determine the uncertainty in the result (R), the measurements of all variables X_i must be independent and repeated measurements of X_i must follow a Gaussian distribution. For practical purposes, the contribution of every measurements to the global uncertainty of a result, can be approximated by the following expression

$$\frac{\partial R}{\partial X_i} \delta X_i \approx \frac{1}{2} \left| \overline{R} - R_{X, \max} \right| + \frac{1}{2} \left| \overline{R} - R_{X, \min} \right| \tag{3.9}$$

where $\overline{R}$ is a result computed with $\overline{X_i}$, *i.e.* the averages of several successive measurements of the variables X_i. The term $R_{X, \max}$ is the same result, computed with the averaged values of the variables, except for $\overline{X_i}$ which is replaced by $\overline{X_i} + s$, s being the standard deviation of the measured variable X_i. $R_{X, \min}$ is similarly computed, replacing $\overline{X_i} + s$ by $\overline{X_i} - s$.

The latest expression described was preferred, in the present work, for its simplicity. Because of the data acquisition system used, it was possible to calculate the standard deviation for measured variables such as X and Y forces, pressure and velocity. For variables with a fix error component, such as length and angles, standard deviations were replaced by reading errors, typically taken to be half the smallest scale division.

In the different figures showing the experimental results, the uncertainty is shown as a typical error bar. These error bars are an average value of errors calculated at different points and they give a general idea of the error on a result. This representation of the uncertainty was used, not to over load the

figures with error bars.

3.4 Procedure

The experimental procedure can be divided into two parts; an installation procedure and a normal run procedure. As the name indicates it, the installation procedure was used when a model was installed on the balance. This only had to be done once, and held as long as the aerofoil was not removed from the balance. The other procedure was used to acquire the data for any specific angle of attack, once the aerofoil was installed.

3.4.1 Installation procedure

When a model was attached to the balance, a small offset angle was introduced between the alignment of the balance and the chord of the aerofoil. This offset angle ϵ was mentioned in section 3.1.5 and the installation procedure was mainly concerned with the measurement of this angle.

The procedure developed was as follow:

1. The balance is installed in the wind tunnel floor and the aerofoil is firmly attached to it.

2. A long square rod is set against the leading edge and the trailing edge of the aerofoil, on the chord, and the balance/aerofoil system is rotated until the rod is parallel to the wind tunnel walls. Then a reference mark is set on the rotating plate of the balance, in line with the zero of the scale fixed on the wind tunnel floor.

3. A system of weights and pulley is used to apply a force perpendicular to the chord of the aerofoil. A string is attached to top of the model, goes out perpendicularly, sits on a pulley, clamped on the side of the working section, and is pulled down by a weight of 2 Kg. A cathetometer is used to make sure that the pulling sting is perpendicular to the wind tunnel walls.

4. The readings of the two components of the balance are recorded, their ratio giving a measure of the offset angle ϵ.

3.4.2 Normal run procedure

Each run was done for a particular angle of attack. To get a complete set of data for each α the model had to be tested twice; once to measure the pressure distribution on the pressure side, and twice to get the one on the suction side. The force measurement was done for each run and the final result was an average of the two set of measurements. This was possible because the collected data was immediately processed into the form of lift, drag and pressure coefficients. The following procedure was used for normal runs.

The model aerofoil was set at the desired angle of attack. A stripe of adhesive tape was put over the pressure holes on the opposite side of the surface scanned. The wind speed was set around the desired level. The information like atmospheric pressure, room temperature, angle of attack of the present run, desired Reynolds number, camber of the model, side of the aerofoil the pressure will be read, frequency of the sampling and time period over which the averages are computed, were entered in the data acquisition system. After a settling period of the wind tunnel, the data acquisition was started. The system measured the force on the aerofoil, the pressure distribution on one side of the model and the wind speed in the tunnel. The wind speed was then fine tuned

41

to get the desired Reynolds number. Time-averaged values were recorded by acquisition system. The same procedure was repeated to measure the pressure on the other side of the model.
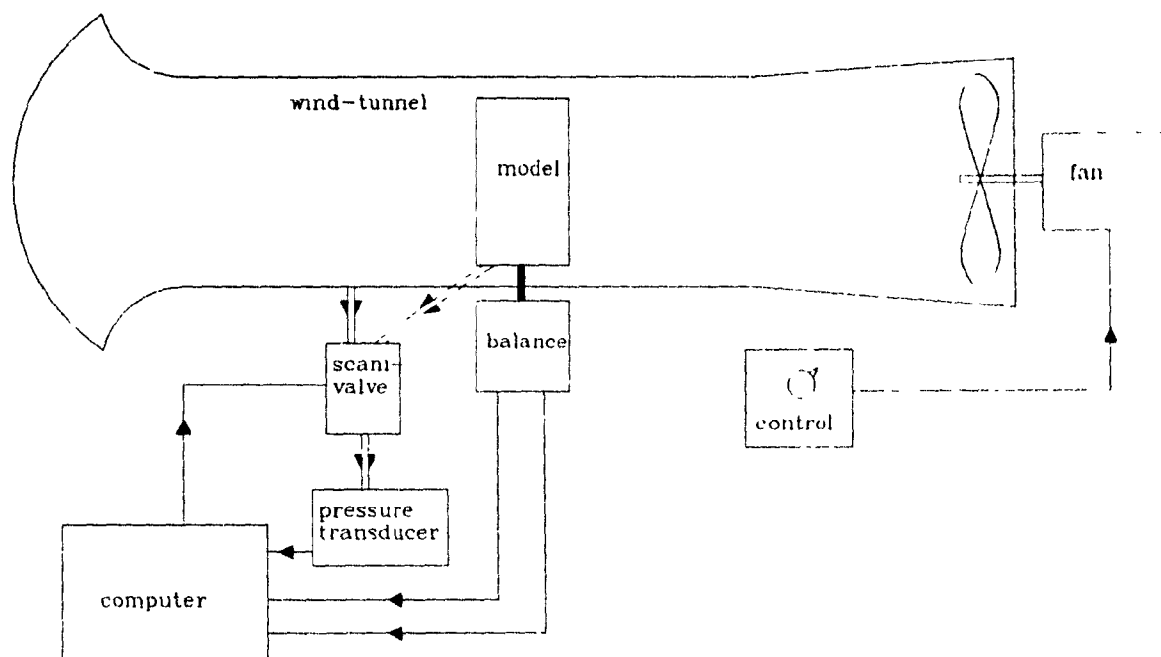
Figure 3.1: Schematic diagram of the experimental set up

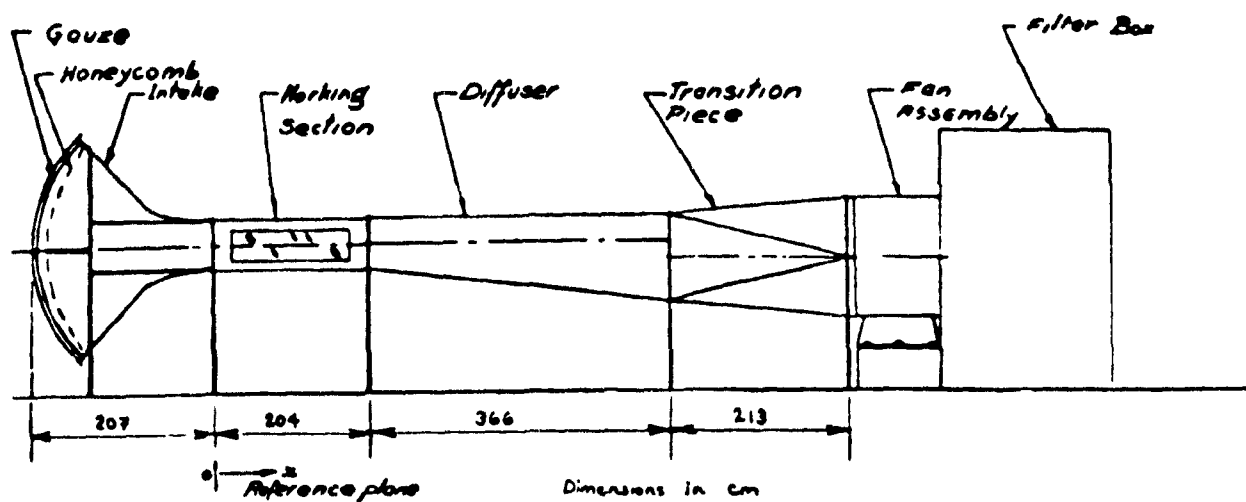Figure 3.2: Photograph of the set up
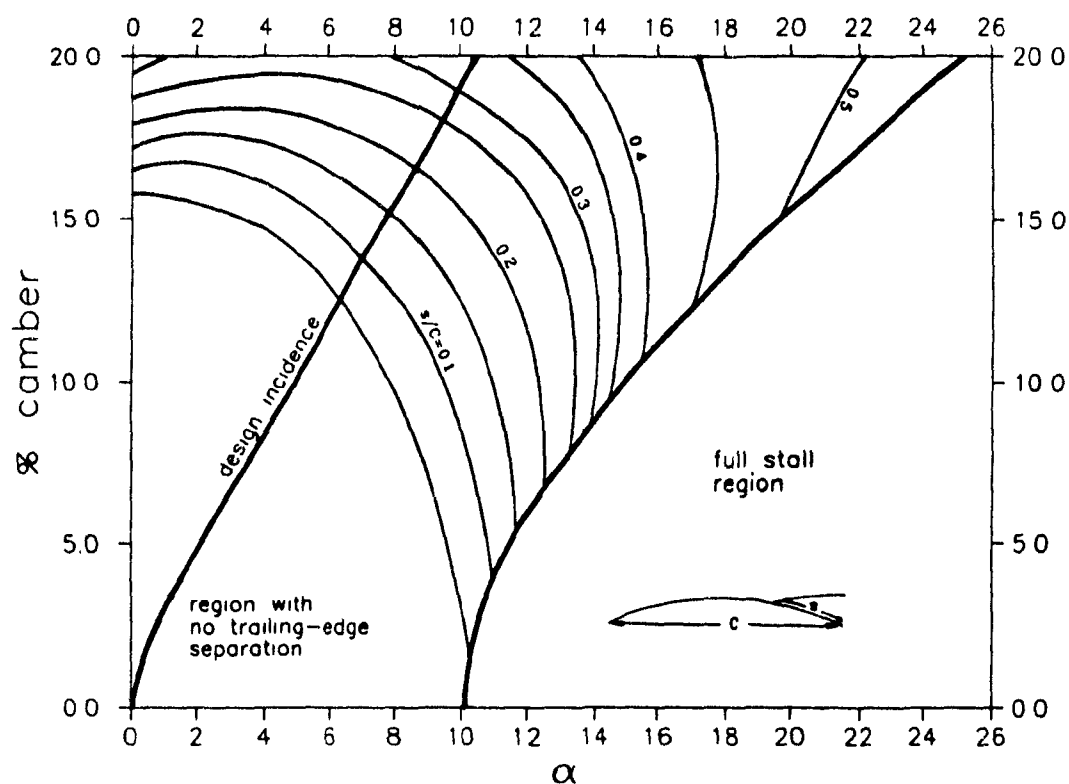
43

Figure 3.3: Diagram of the wind tunnel

Figure 3.4: T.E. separation (measured from the t.e.) for circular-arc aerofoils as a function of camber and α. Tests done in the smoke tunnel at $Re = 3.5 \times 10^4$

44
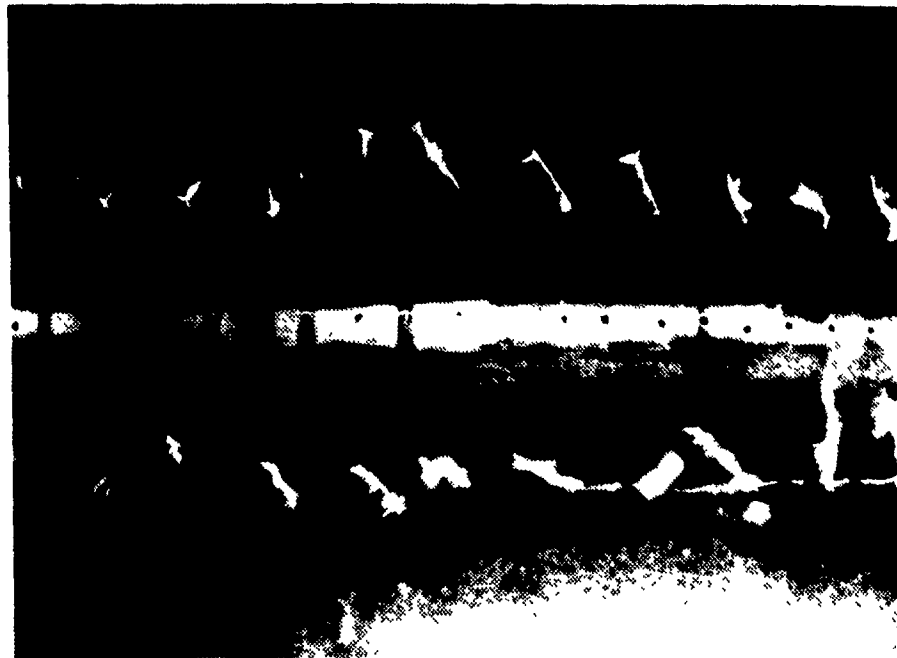
Figure 3.5: Close up photograph of the pressure taps. Plan view of the centre of the aerofoil (the tufts are shown with wind off).
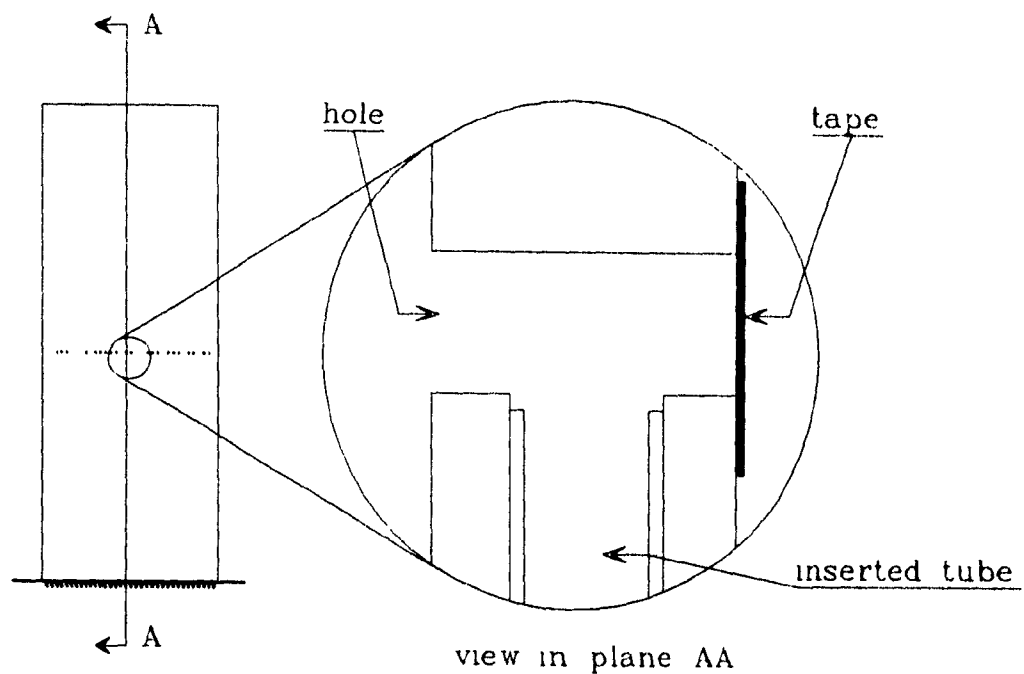
view in plane AA

Figure 3.6: View in plane AA of the pressure tap: left hand hole opened, right hand hole closed.

45
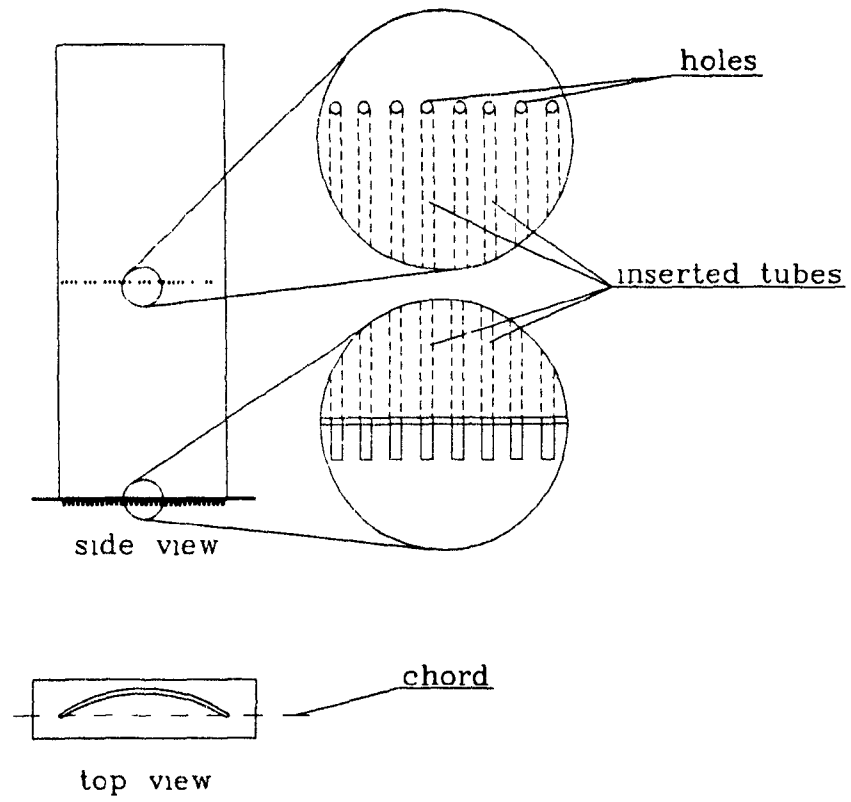
Figure 3.7: The circular-arc aerofoil

Figure 3.8: Photograph of the 18% cambered model
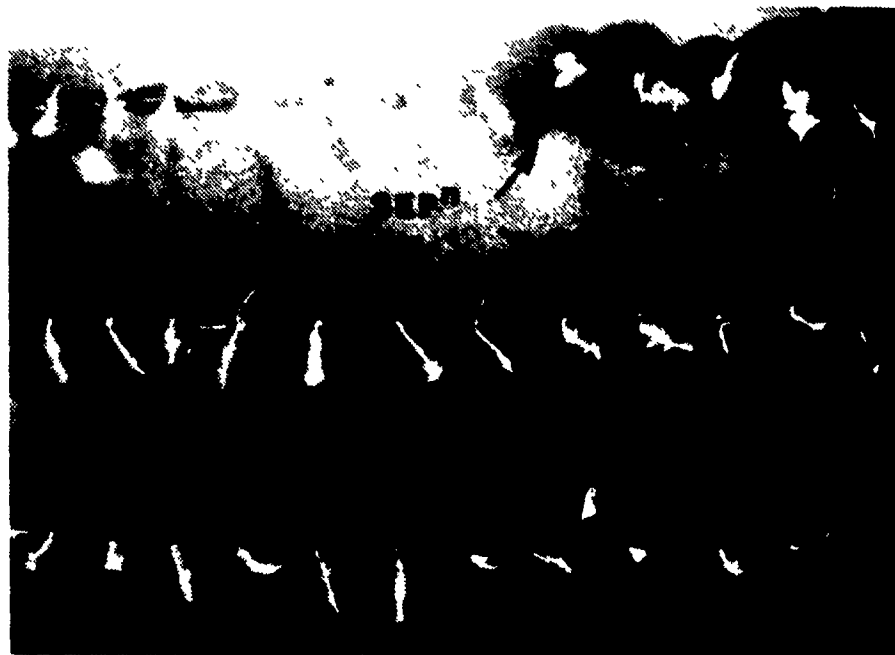
Figure 3.9: Close up photograph (wind off) of the tufts and the traces left by the flow
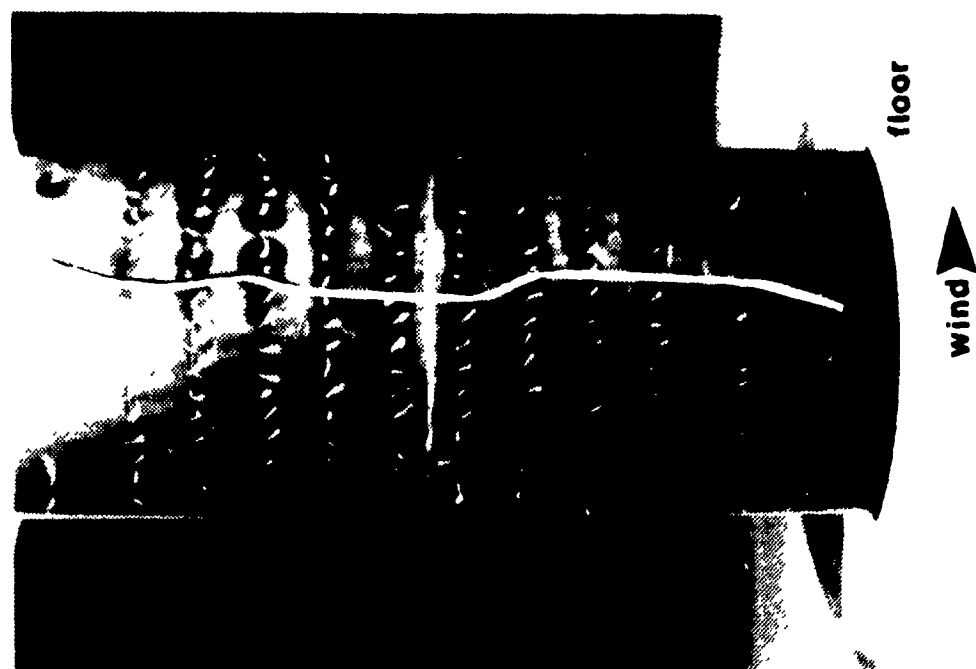
Figure 3.10: Tufts used to show flow separation. Separation is shown by the white line.
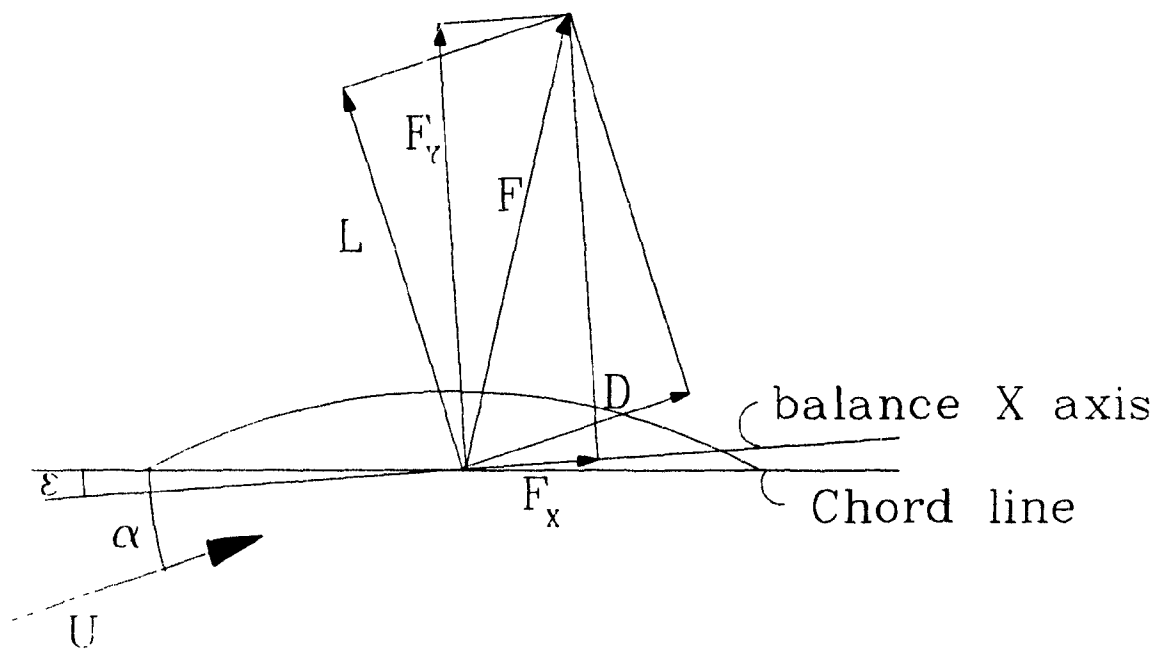
Figure 3.11: Force diagram
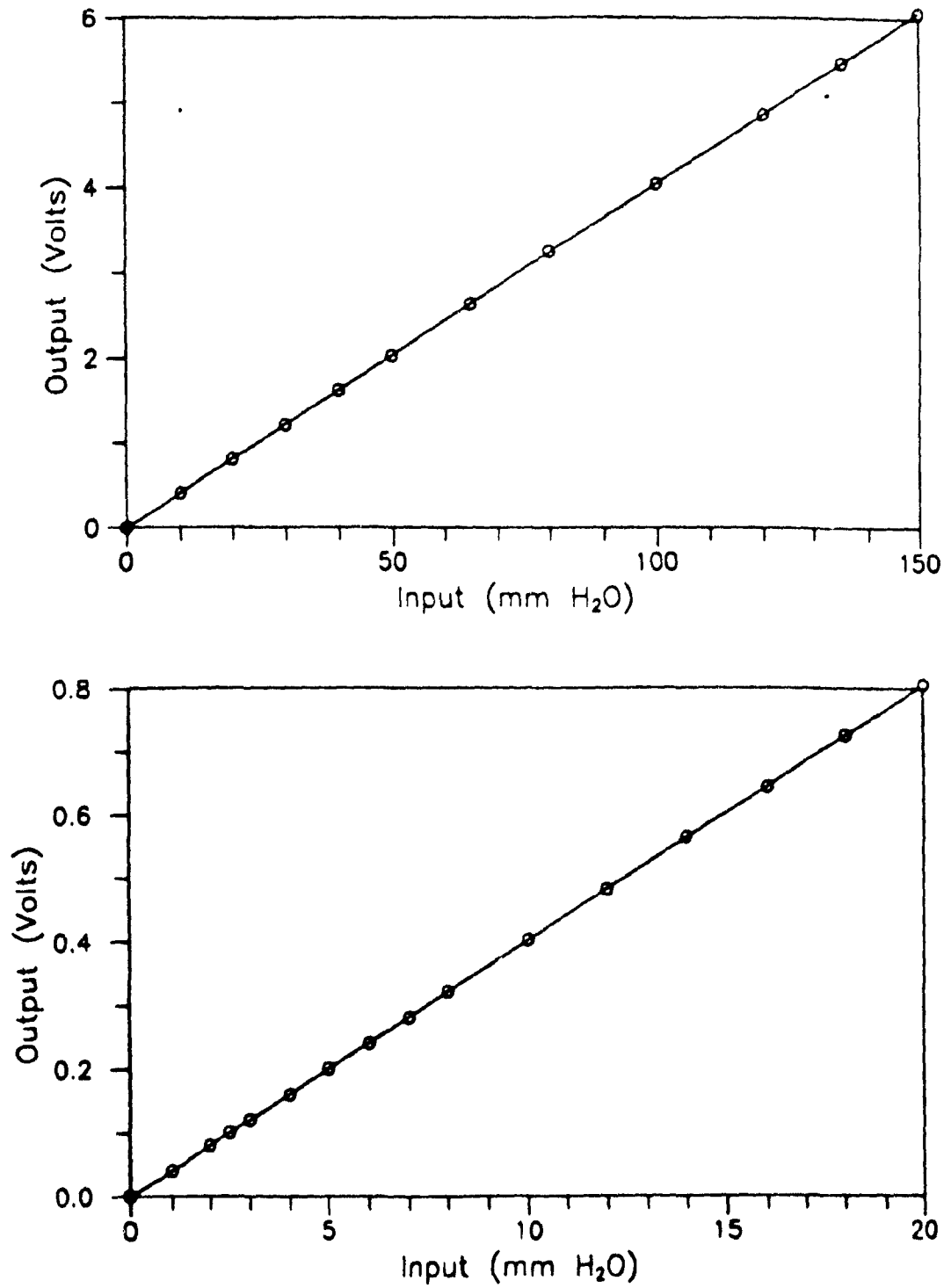
Figure 3.12: Calibration curve of the pressure transducer (Barocel)

Chapter 4

Results and Discussion

This chapter first discusses details of the theoretical model. Several elements of the experimental part of this research are then discussed. Finally, the experimental results and the results of the simulation are compared to see if the theory is a plausible method of prediction.

4.1 Numerical model

4.1.1 The closure conditions

In the final form of the mathematical model, four hypotheses are used as closure conditions. In chapter 2, a description of these hypotheses is given. A small discussion on the role of each of them is given here. The closure conditions are named as follows

1. Kutta condition

2. Design incidence condition

3. Base pressure hypothesis

4. Lift hypothesis

The Kutta condition (see section 2.2.1), directly identifies the circulation needed to make the whole potential flow realistic. It ensures that the flow about the aerofoil has qualities found on real aerofoils; a finite pressure at the trailing-edge and streamlines that resembles what can be observed experimentally.

The design incidence condition (see section 2.2.2) brings information about the angle of attack. For circular-arcs, angles of attack other than the design incidence are undesirable. They are because leading-edge separation bubbles would be formed [8] and the prediction of the turbulent boundary-layer after reattachment would be difficult [1]. This is why the design incidence is sought.

The first two conditions are classical. The third condition, the base pressure hypothesis (see section 2.2.3), has an approximate counter-part for viscous flow which is described in Thwaites [17]. This condition uses a boundary-layer calculation that provides an information on where a real flow would separate in the pressure distribution given by the potential flow. This part of the calculation brings in new information. The quality of this information is related to the quality of the boundary-layer method used and to the assumptions made using the method. The method of Head and Patel seems to give good results for different bench mark simulations [3] and the major assumption made in the present model, is to neglect the effect of the curvature on the evolution of the boundary-layer. Some assumptions were also made to find the initial conditions on the momentum thickness and the shape factor, but these have been found to have a small effect on the calculations (see section 2.3.1).

The information brought by this condition helps to determined the strength of the source, i.e. the amount of injection. Using this condition, the overall

51

pressure distribution is modified to get closer to a real distribution. As the pressure distribution is improved, the prediction of the point of separation gets better.

A last condition is needed to fix the position of the source. This condition (see section 2.2.4) uses the lift that can be obtained from the potential flow. The circulation, Γ, is one of the variables in the potential equation and the lift is directly related to it. This circulation is mainly influenced by the first condition, but it is refined by the third one. The finer adjustment is done by making sure that the lift obtained from circulation, in the potential flow, is consistent with a lift computed from the integration of a realistic pressure distribution found all around a separated aerofoil. This pressure distribution is the one obtained from the potential flow with a constant "base pressure" part from the separation point to the trailing-edge. This modified distribution is very similar to a real one (see fig. 4.1), hence the lift obtained from its integration is reasonable. By modifying the position of the source, the circulation lift and the pressure lift are brought into agreement. In other words, the fourth condition fixes the value of the base pressure so that the two different ways of computing the lift agree, making sure that the circulation is related to a plausible lift.

It has to be clear that this theory is considering three different values of lift. Two of them are coming from the simulation and the third one is the real lift of a circular-arc aerofoil at design incidence with separation. In the simulation, one lift comes directly from the circulation in the potential flow. The other comes from the integration of the modified pressure distribution. The pressure distribution is modified to fit more closely a real pressure distribution and this is where the linkage is made between the simulation and the real flow. The lift obtained from the modified pressure distribution is directly related to the real lift as a consequence of the similarity between the real pressure distribution and the modified one. The last condition is used to force an agreement between the

52

two lifts of the simulation (circulation, modified pressure distribution) because such an agreement exists on a real aerofoil *i.e.* the lift computed from the measured pressure distribution is equal to the lift found from the circulation around the aerofoil. This condition indicates that a realistic modified pressure distribution has been found. The real lift is never used in the model, only the measured pressure distribution was used qualitatively to justify the last condition.

The effects of the closure conditions have been described in steps. But when incorporated in an iterative scheme, each condition are satisfied sequentially. Each step brings a variable closer to its converged value until at convergence, all conditions are satisfied simultaneously. Then the simulated flow is considered to have enough similarity with a real flow to give useful information.

4.1.2 The separating streamline

From the stagnation point appearing in front of the source on the extrados of the aerofoil, a streamline leaves the aerofoil. As it is expected in potential flow, this streamline leaves the surface at a right angle. But the streamline curves rapidly in the direction of the main flow and the part of the streamline leaving at wright angle is hardly noticeable compared to the size of the aerofoil. This streamline cannot strictly speaking be associated with the separating streamline found on a real aerofoil, simply because it does not leave the aerofoil from the calculated separation point but from a stagnation point. In fact, in the theoretical model, no streamline leaves the aerofoil from the calculated point of separation. This does not seem to be an essential requirement for the model to give realistic predictions.

4.1.3   Incorrect prediction of drag from sources

The first iteration scheme that was designed used the five closure conditions described in the theory. Using these, it became obvious that the whole scheme was converging to an inadequate value of source strength from which it was impossible to simulate properly the pressure distribution around the aerofoil. The condition on the drag was requiring an amount of injection lower than what was needed to simulate adequately the lowest pressure on the aerofoil. It then became clear that the hypothesis on the drag seemed to be inexact. This was not surprising since the drag hypothesis was likely to be erroneous.

One assumption likely to be incorrect, is that the momentum loss thickness was approximated by the displacement thickness in the far wake of a separated aerofoil. Because of the presence of a large region of separation containing back flow, there is a big deficit in the velocity profile leaving the aerofoil. If the velocity profile in the far wake has a small deficit compared to the free-stream velocity, then it is reasonable to assume that the definition of the momentum loss thickness and the definition of the displacement thickness are giving approximately the same result. But if, as was mentioned above, the deficit is initially large it is probable that in the far wake the momentum loss and the displacement thickness are not sufficiently equal.

Because of the use of the boundary-layer calculation, the sources in the model are primarily needed to influence the pressure distribution. In the drag hypothesis, the injection due to the sources is used to simulate the momentum loss associated with the drag of the aerofoil. It was then implicitly assumed that the loss of momentum alone, was responsible for the modification of the pressure distribution. One can see that if it is not the case, the same amount of injection will not be able to give the right pressure distribution and a good estimate of the drag at the same time. So it is believed that the modification

of the pressure distribution due to the viscous losses and the separated region, may not be solely related to the loss of momentum.

4.1.4 Prediction of separation from B-L calculations with pressure distribution that leads to a stagnation point

The boundary-layer calculation used in this numerical model, uses the pressure distribution over an aerofoil to predict the position of separation. In the neighbourhood of separation, the calculations are very sensitive to small changes in the pressure gradient. If the actual pressure distribution measured on the 18% cambered aerofoil, at design incidence, is used to calculate the boundary-layer development, it is observed that the calculations does not predict any separation. This was also observed by Güven et al [2] who used measured pressure distributions on a circular cylinder in a boundary-layer development to see if separation could be predicted. However, they found that if the pressure distribution in the neighbourhood of separation is extrapolated along the adverse pressure gradient there, then separation is predicted some distance downstream of the measured separation. Hence in order to calculate a point of separation from the measured pressure distribution on the 18% circular-arc aerofoil, the pressure distribution would have to be extrapolated beyond the real point of separation using the pressure gradient found there as shown on figure 4.1 by the dotted line.

In the present model, the calculations of the boundary-layer development are based on the pressure distribution obtained from the potential flow, not from a measured pressure distribution. The useful portion of the distribution goes from the leading-edge to the stagnation point in front of the sources. If the extrapolated experimental pressure distribution (dotted line) is compared to the

one obtained from potential flow, one can notice that the pressure distribution obtained from potential flow naturally extends beyond the experimental point of separation. Another important point to notice is that the potential pressure gradient increases past the experimental point of separation. This increase in the pressure gradient, compared to the constant experimental extrapolation proposed by Güven *et al.* [2], helps to predict an earlier separation. Hence, the pressure distribution obtained in front of the sources suites the needs of the boundary-layer development method to predict separation.

4.1.5 A distribution of sources compared with a point source

Basically two different kind of sources can be used to represent the separated region. There is the normal point source which has no dimension and which is fundamentally, in two-dimensional flow, a volumetric injection of fluid per unit width. The other kind is a distribution of sources. In this configuration the source has no thickness, its length is infinitesimal and the fluid is injected at a constant speed at the surface of the source. Using these sources, it is possible to make a continuous distribution of sources on any path or surface.

The theoretical model was developed using the second kind of sources, mainly for two reasons. The first one came from the fact that Newman and Tse [8] used a constant distribution of sources to simulate, with good success, the effect of the leading-edge bubble separation on a flat plate. The argument is based on some similarity found between the velocity profile over a separated region (ignoring the back flow part) and the one found in a free shear layer. Because the mixing region of a turbulent free shear layer grows linearly with distance, some constant injection velocity can be related to that growth. Hence if the two velocity profiles are somewhat similar, it is reasonable to assume that

the same injection velocity can be associated to both of them. This injection was provided in the potential flow field by a uniform distribution of sources.

The second reason was to develop a numerical model with flexibility. If a uniform distribution of constant sources is used to inject a finite amount of fluid in a flow, and if this amount is kept constant as the length of the distribution reduces to zero, the distribution of sources becomes a point source. Hence it is possible to obtain the effect of the first kind of source using the second kind. The use of elemental sources made it possible to test the numerical model with different strength distributed over a finite length and, in the limit, with a point source.

4.1.6   The model and the computer

The calculations were performed on a 80386 DOS based machine running at 33 Mhz with a maths coprocessor. Using reasonable initial guessed values for the strength of the source and its position, the calculations were done in a couple of iterations and they took about 2 minutes to converge to the final solution.

4.1.7   advantages and disadvantages of the model

The main advantage of the numerical method its simplicity. The separation was predicted and compared with experimental measurements only for the 18% circular-arc. But nothing in the conception of the model restricts its application to circular-arc aerofoils. A separation on any other aerofoil could be predicted if only the potential flow around the aerofoil, with sources in the separated region, could be provided. The solution would be composed of essential information about the aerofoil, namely the pressure distribution around it, including the base pressure, the circulation and the point of separation. From these it

57

would be possible to get the lift and the pressure drag, and if a boundary-layer calculation was included all around the aerofoil and its results integrated, it would be possible to add the friction drag to get an evaluation of the total drag. The solution would be obtained rapidly and could be performed on a micro-computer. The method was developed for two-dimensional aerofoil but it could probably be used as design tool to predict the position of separation on wings of high aspect ratios near the stall.

On the other hand, the proposed numerical method cannot predict the behaviour of an aerofoil at any angle of attack. It can only handle flow with a trailing-edge separation alone, which limits its range of validity. It is also limited to handle low Mach number flows.

4.1.8 The use of the method for aerofoils other than circular-arc aerofoils and at other angles of attack

The numerical method developed in this thesis is design to only take into account the trailing-edge separation of an aerofoil. For circular-arc aerofoils, if there is a trailing-edge separation, there is always another separation bubble at the leading-edge except at design incidence. This is why the design incidence was studied for this research. But for aerofoils having a rounded leading-edge, there can be a whole range of angle of attack for which there is a trailing-edge separation without any leading-edge separation. In that case the angle of attack would become a specified variable in the problem and the condition on the design incidence would be dropped. The sources would still play the same role, *i.e.* provide the right pressure distribution to the boundary-layer calculation and the other hypotheses would still be valid, because they apply to any aerofoils with separation. Hence it is reasonable to assume that the model would give good results not only for the design incidence but for a whole range of

58

angles of attack, as long as there is no leading-edge separation.

4.1.9 Drag calculations

Because the condition on the drag was abandoned, it is not possible to relate the total drag directly to the amount of injected flow by the sources. But the simulated pressure distribution with the modified constant part from separation to the trailing-edge gives a good simulation of the real pressure distribution measured on the 18% circular-arc aerofoil. This pressure distribution integrated around the aerofoil gives the pressure or form drag.

4.2 Experimental work

4.2.1 Design procedure for the choice of the circular-arc camber

The main design requirement for the experimental aerofoil, was that the flow had to have a relatively large separated region at design incidence. A separated region of 25% the size of the chord was considered sufficiently large to be clearly measured. Available data obtained on small circular-arc aerofoils [18], indicated that a 10% cambered aerofoil would fulfil the requirements. A 10% cambered aerofoil was built but when it was tested, it showed no sign of trailing-edge separation at design incidence. Clearly the available data on the separation position on circular-arc aerofoils was incorrect and no other data was found. So a series of tests were done on aerofoils of 0%, 5%, 7.5%, 10%, 15% and 20% for angles of attack ranging from 0° to full stall. The tests were done in a smoke-tunnel ($Re = 3.5 \times 10^4$) in order to measure accurately the design

incidence. Tufts were glued at the surface of the aerofoils and they were used in conjunction with the smoke to determined the position of separation. All the data obtained was fed into a contour plotting software to give figure 3.4. Using this contour plot, an 18% cambered aerofoil seemed to meet the specified design requirements. This contour plot can only be used as a rough estimate of the behaviour of the larger aerofoils in the 3×2 wind tunnel, mainly because:

- The Reynolds number in the smoke-tunnel was around 3.5×10^4 which was much less then the intended Reynolds number (4.0×10^5).

- The aspect ratio of the aerofoils used in the smoke-tunnel were very different, 0.75 compared to 2.65 for the larger model.

- The blockage effect due to the aerofoils sizes compared to the cross-section dimensions of the smoke-tunnel was not negligible, but no correction could be calculated since no force measurements were made in that tunnel. Another effect of the tunnel, is the influence on the angle of attack. This influence varies with the circulation around the aerofoil. Hence, on figure 3.4, the design incidence is probably closer to reality than the incidence for full separation.

4.2.2 2-D or not 2-D, that is the question

Because the numerical model represent a two-dimensional flow over an aerofoil, care was taken to design experiments that would produce as closely as possible a two-dimensional flow over the experimental aerofoils. The span was more than twice the chord and the aerofoil was extending from the floor to the ceiling of the wind-tunnel. The observation of the tufts glued at the surface of the aerofoil gave useful information on the behaviour of the flow. Tufts were easy to read in the steady parts of the flow and, using a powdered surface, it became fairly

easy to get a clear picture of the time-averaged behaviour of the flow in the unsteady regions.

For the two cases tested, the 10% and the 18% model, a separated region larger than the mean separation was always present at the trailing-edge, against the floor of the wind tunnel. This region combined two boundary-layers, the one on the wind-tunnel floor and the one on the aerofoil. The combined effect of the two boundary-layers explains the presence of this larger region. A similar region was expected at the ceiling of the tunnel but was not found. The aerofoil was only attached by one end, on the balance, at the floor of the tunnel. The other end of the aerofoil was very close to the ceiling of the wind-tunnel but did not touched it, there was a small gap between the two (about 3 mm). Because there was a high pressure on one side of the aerofoil and a low pressure on the other side, air flowed from the high pressure side to the low pressure one. Doing so the boundary-layer at the ceiling was energized and the interaction between this energized boundary-layer and the one on the aerofoil was different from the interaction at the floor. The gap at the free-end of the aerofoil was large enough to let air flow but too small to allow the development of a large vortex structure. Hence this gap made the flow closer to a 2-D flow near the ceiling.

A large end-plate was tested close to the floor to isolate the aerofoil from the boundary-layer of the wind-tunnel, which had a thickness of approximately 3.8 cm (1.5 in) at the level of the aerofoil and for the speed at which the tests were ran [20]. The end-plate was attached to the aerofoil at 3.8 cm (1.5 in) from the floor. This plate reduced by a little the size of the separated region observed near the floor. But this reduction had no influence on the measurement of the lift and because the plate was attach to the balance, the drag was significantly increased. To get an isolated value of the drag for the aerofoil, measurements of drag on the end-plate alone would have been necessary. By substraction of the drag of the plate from the total drag of the aerofoil-plate assembly, it would

61

have been possible to evaluate the drag of the aerofoil alone. But by adding steps in the procedure to get the drag, sources of error would be added and for a quantity as small as the drag, the error in the measurement has to be kept as small as possible. It was then decided to abandon the use of an the presence of the plate significantly increased the drag. It was then decided to abandon the use of an end-plate considering that the small improvement on the flow was not detectable on a measured quantity like lift and to keep the procedure to obtain the total drag as simple as possible.

The observation of tufts was the only tool used to get an idea of the two-dimensionality of the flow. It is not an excellent test to determine if the flow is two-dimensional but it reveals the presence of three-dimensional structures in the flow. For the 10% circular-arc, the tufts were all mostly in the direction of the main flow for all the angles of attack tested. The flow behaved differently in the regions soaked in the boundary-layer of the wind-tunnel, but the deviation from the constant trend found in the central part of the aerofoil was slight. The tufts on the 18% aerofoil, showed evidence that the flow was not perfectly two-dimensional for a certain range of angles of attack. It is mostly the line of separation that was used as a sure indication of three-dimensional effects. When the leading-edge bubble was absent or very small, the spanwise position of separation was not found on one straight line but rather on a zigzag line. The length of some indentations were as big as 1/6 of the chord length at the design incidence. As the angle of attack was increased, these indentations reduced in length and for large angles of attack, the line of separation was found to be very straight. When the angle of attack is close to the design incidence, the flow at the leading-edge is laminar and after a short distance it transits to turbulent. The air in this turbulent boundary-layer follows the surface of the aerofoil and when it encounters a pressure gradient that is too large, it leaves the surface and flows over the region of high pressure. But because the surface of the aerofoil is not perfectly smooth and not perfectly curved, the spanwise

position of separation does not occur at the same chordwise distance. When a stream of air separates from the aerofoil, it modifies the structure of the flow locally which changes the pressure and a neighbouring stream separates at a slightly different chordwise position. When the angle of attack is increased, a separation bubble is formed at the leading-edge and when the flow reattaches it is much more turbulent than if it had developed from an attached laminar boundary-layer. This flow being more turbulent, the mixing is also increased which evens out the spanwise effect of separation and on a time-averaged basis the separation line is straighter.

Finally the best indication of the two-dimensionality of the flow was found in the agreement between the lift measured on the balance and the lift obtained by integration of the measured pressure distribution. Since the measurement of the balance is giving an averaged value of the contribution of the whole span of the aerofoil and the measured pressure distribution is localized only at the mid-span, the agreement between the two measurements is an indication of two-dimensionality. Figure 4.8 shows the curves for the two different aerofoils and it can be noticed that the agreement between the two different measurements is very good for both aerofoils.

4.2.3 Choice of Reynolds number

It was mainly for practical reasons that the tests and the simulation were run at a Reynolds number of 4.0×10^5. The Reynolds number had to be sufficiently high to make a comparison with the results obtained by Wallis [19] at Reynolds numbers of 3.14×10^5 and 4.08×10^5. Some tests were done to try to find the maximum Reynolds number for which a whole range of angles of attack could possibly be tested. Because the experimental model was fixed to the balance at one end only, at dynamic pressures corresponding to Reynolds numbers of

the order of 5.0×10^5 heavy vibrations began to appear on the 10% model at angles of attack few degrees above the design incidence. For the same model, at higher angles of attack $(\alpha = 12°)$ the force measurements were getting close to the limits of the available balance. Tests were run at $Re = 3.0 \times 10^5$ and the lift and drag curves were very similar to the parts of curves obtained for $Re = 5.0 \times 10^5$. It was then decided to run the tests at an intermediate Re, i.e. $Re = 4.0 \times 10^5$, not to exceed the limits of the balance and to avoid large vibrations of the models.

4.2.4 Validity of the experimental results. Comparison with Wallis' results.

A circular-arc is not usually a useful aerofoil. Because it has negligible thickness, high pressure gradients are present at the leading-edge that generate separation bubbles which reduce the lift and produce more drag. For highly cambered aerofoils, separation appears easily at the trailing-edge which further reduces the lift and leads to even more drag. This mainly explains why circular-arc aerofoils are not generally used in practical applications except maybe for economical blades. As a consequence, there are very few experimental data available on circular-arc aerofoils.

The only data found by the author, is due to Wallis [19]. It includes the lift, drag and quarter chord moment for aerofoils ranging from a flat plate to 10% cambered circular-arc. The lift was measured with a mechanical balance and the drag was calculated from wake traverse measurements. Wallis' results for the 10% cambered circular-arc were compare to the present results to show if there were any errors in the procedure used in this research.

Comparing the two results, it is noticed that neither the present curve

for the lift or for the drag falls over Wallis's. Looking at the drag curves, presented on figure 4.2, one can see that the present results are shifted to the left. The minimum drag is shifted by about 2.6° and for larger angles of attack the shift seems greater. Translating the present drag curve to the right by 2.6°, fits the two curves more closely. Those two curves were obtained by two completely different methods. Wallis used pitot traverses to determined the profile drag. These methods, based on the total pressure measurements in the wake, are known to give very accurate results if no separation is present on the aerofoil[14]. For small angles of attack certainly no separation regions were present but for angles of attack larger than the design incidence, separation was certainly present. Wallis' results are then more doubtful for large angles of attack where the disagreement is the largest between his results and the present ones. The total drag in the present results was measured from the vectorial decomposition of two perpendicular balance measurements in the main flow direction. The drag is a small quantity compared to the lift, and using this method, it is the result of the subtraction of two comparatively large values. This result is very dependent on the actual direction chosen to recompose the vectors. An error of only 0.5° in the direction can give an error on the result of more than 75%. For the calculation of drag from the recombination of two balance measurements, there are two possible sources of error in the direction. The first one is the interference of the wind tunnel on the model and the second one is the offset between the chord of the aerofoil and the alignment of the balance. Because the computation of drag using a traverse measurement of pressure in the wake is effectively independent of any angles, the agreement between the two drag measurements shows that the possible sources of error, for the balance measurements, have been taken into account.

Another clue which indicates that the procedure for obtaining the drag is correct, comes from the comparison of the total drag curve and the pressure drag curve 4.2. The pressure drag is always lower than the total drag, which is

normal, but more the two curves tend to follow the same trend. The pressure drag measurements are pretty well independent of the alignment between the chord of the arc and the balance. This then shows that the offset alignment is correctly measured. The small discrepancy appearing for angle of attack larger than 6° is due to the appearance of a peak of very low pressure at the leading-edge at these angles of attack and no pressure tap is close enough to the leading-edge to properly measure this peak.

An offset difference of 2.6° is relatively small compared to the chord size of the models (22.86 cm (9 in.) in the present research and 15.24 cm (6 in.) for Wallis). An offset in the reference line of the wind-tunnel is probably responsible for this difference. In this research, a reference line was set for each model using a square rod 1 m long. The rod was set against the leading and trailing edges of the circular-arc and the aerofoil was rotated until the rod was perfectly parallel to the walls of the wind tunnel. A reference line was then marked down on the rotating plate, in line with the zero of the scale.

The lift is an easier quantity to measure. As opposed to the drag, the lift is the result of the addition of two vectorial components. It has a much larger value than the drag and it is not very sensitive to offset direction. Here again, it can be noticed from figure 4.3, that the present results do not fall on those of Wallis. There is a shift, of about 0.5° to ..'e right, of the present results. Again if the two curves are superimposed one on top rf the other, the agreement is very good. Because there is no indication in Wallis' report on how the lift was obtained from the balance, it is difficult to explain why the lift curve is shifted in the other direction. Presumably it comes from the same sources, *i.e.* an incorrect reference line in the wind-tunnel and misalignment of aerofoil with the balance. Since the present drag results are in perfect agreement with results based on a method independent of alignment angles and because the calculations of the present lift are less dependent on those misalignments then

the drag, the present lift results are considered to be valid. There are no data available for an 18% cambered circular-arc aerofoil. Therefore it is not possible to compare the present data obtained for the 18% model with any other data. But the procedure used the get the data for the 18% case is exactly the same as that used to get the data for the 10% case. Hence the present results for the 18% case are also considered to be valid.

4.2.5 Effect of leading-edge shape

The first experimental models tested had a wedge shaped leading-edge. The angle of the wedge was 45° which made the leading edge very sharp. Because of this configuration, the lift curve has a peculiar behaviour (see figure 4.4). For angles of attack lower than $-1.5°$ the lift curve tends to have a high slope (larger than 2π). Above $-1.5°$ the curve is again linear but the slope is much less. This change in the behaviour of the lift curve can be explained by the effect of the leading-edge separation. Around $-1.5°$, the stagnation point at the leading-edge is situated on the extrados of the aerofoil which produce a separation bubble underneath the aerofoil. Below $-1.5°$, this bubble is very large and encloses most or all of the aerofoil on the intrados. In that case, the streamlines underneath the circular-arc have a curvature opposite to the one of the arc. Above this limit, the bubble still exists underneath the aerofoil but its size is now suddenly reduced. This has the effect of changing the curvature of the streamlines. They are then curved in the same way the circular-arc is. Those two different configurations of the flow around the circular-arc seem to be at the origin of the difference in behaviour of the lift line.

Two different slopes are present on Wallis' lift curve but the very sharp change, from one to the other is not observed because Wallis used a rounded leading-edge. The leading-edge of the present experimental models were rounded

by wrapping them with a very thin adhesive tape. This had the effect of eliminating the sharp change of slope and the lift curve obtained is very similar to the one obtained by Wallis (see fig. 4.3).

4.2.6 Transition to turbulence

For angles of attack around the design incidence, an additional measurement was made. A small Pitot tube facing the flow was mounted on a traversing system and brought to the upper surface of the aerofoil. The Pitot tube was connected to a stethoscope to detect the position of transition on the aerofoil. The distance to transition was nearly constant on the central section of the aerofoil, but it decreased in regions close to the floor and to the ceiling of the wind-tunnel. The transition distance for the 10% model was around 5% of the chord length for a $Re = 4.0 \times 10^5$. For the 18% model the transition occurred at 8% of the chord for the same Reynolds number. The starting position used in the numerical simulation is based on a transition on a flat plate and is at 10% of the chord after the leading-edge. But as was mentioned earlier, the prediction is not very sensitive to that position.

4.2.7 Separation point evaluation

The position of separation on the aerofoil was determined using the tufts. Separation on a real aerofoil, specially turbulent separation, is not a steady process. The line of separation is always moving back and forth around a mean position. This position is not easy to evaluate just be looking at the tufts and the interpretation could depend on the observer. This is why the surface of the aerofoil was covered with powder to record the time-average behaviour of the tufts. The tufts were distributed on 13 rows and the separation was recorded for each

row. An average was then computed to obtain a mean position of separation. The tufts were 1.3 cm (0.5 in) apart from each other on the rows. This spacing may seem large to measure separation accurately but it is considered to be sufficient. The tufts must have a minimum room to move and considering the unsteady process they are measuring, it is believed that an average of several measurements gives a good evaluation of the separation position.

The position of separation may also be estimated by looking at the pressure distribution around the aerofoil. It is chosen to be the point, near the trailing-edge, where the pressure starts to be constant. But this point is not very precise since the pressure does not become exactly constant as you get in the region of separation (see fig. 4.5).

4.3 Comparison with the present theory

The different predictions, obtained from the theoretical model, are now compared with the experimental results. As mentioned before, the comparison is only done with results of the 18% cambered aerofoil. Even though the only experimental results needed are the ones measured at design incidence, a large portion of the experimental results obtained in the present work are presented in this section.

4.3.1 Pressure distribution and base pressure

The most important element of the simulation, is the prediction of the right pressure distribution; because two closure conditions are based on this distribution. Figure 4.5 shows a fairly good agreement between the simulated and the measured pressure distribution. The peak negative C_p is a bit out. The

69

pressure at the point of separation found by the boundary layer calculations, is taken to be the base pressure and set constant up to the trailing edge. This predicted base pressure is found to be very close to the experimental value.

From the measured pressure distribution, the position of separation is estimated as follows. The pressure points on the suction side are characterised by a set that varies and a second set which is constant near the trailing-edge. A line is fitted through the data of the base pressure, giving a straight line and a curve is fitted through the other data points. The point of separation is at the intersection of the two curves. The predicted separation compares very well with this definition of the experimental separation point.

The effect of the circular-arc thickness

The numerical model calculates the pressure distribution on a circular-arc aerofoil. The aerofoil obtained using conformal transformation has theoretically no thickness. For practical reasons, it is impossible to build such an aerofoil and the experimental models used had a thickness to chord ratio of 1/72. To see the effect of the thickness alone, the potential flow around a very slender Rankine oval of thickness to chord ratio of 1/72 was studied. Figure 4.6 shows that for such an oval, there is a minimum pressure located close to the leading-edge and the trailing-edge. Hence a circular-arc aerofoil having some thickness will have a lower pressure on both sides of the aerofoil near the leading-edge and the trailing-edge. The effect of the thickness can be seen on the pressure distribution around the aerofoil. Looking at figure 4.5, it can mainly be noticed on the pressure side at the leading-edge and at the trailing-edge of the aerofoil. There is no noticeable evidence of this effect on the suction side at the leading-edge. At the trailing-edge the mixing due to the turbulence in the separated flow evens out the pressure, erasing this effect. Because it is relatively small and localized, the effect of the thickness was not incorporated in the theoretical

70

model.

4.3.2   Separation point and design incidence

The separation point was measured experimentally in two ways. The first one was described in section 4.3.1 but it only gives a position of separation at one spanwise location. If the flow was perfectly two-dimen͘͘͘ the position of separation would be the same for all spanwise positions But because of small three-dimensional effects, separation does not occur on a straight line. Hence the position of this separation line was measured for all spanwise positions with the tufts glued on the surface of the aerofoil. From these measurements an average was computed to give an effective 2-D chordwise separation position. An average separation position was measured at each different angle of attack and the results can be seen in figure 4.7.

The predicted position of separation is found on this figure at the predicted design incidence. Both prediction are close to the experimental values and fall within the experimental error.

4.3.3   Lift

The lift curve of the 18% circular-arc aerofoil is presented in figure 4.8. It can be noticed on the figure that the experimental pressure lift is in very good agreement with the lift measured on the balance. The predicted lift at design incidence is also fairly close to the experimental value. It falls within the experimental error region indicated by the cross on the figure. The agreement between the pressure lift and the lift measured on the balance is also very good. As was mention in section 4.2.2, this is taken as a sign of good two-dimensionality of the flow for both aerofoils.

The lift curve of the 10% aerofoil shows clearly two different slopes. A possible explanation was given by the change in effective camber as the incidence is increased. The first part being dominated by the presence of a leading-edge bubble on the intrados of the aerofoil and the other part by a trailing-edge separation. On the 18% aerofoil there is no clear distinction of two slopes because the design incidence ($\alpha = 6.5°$) — where the leading-edge bubble disappears — is very close to the stall. The part of the lift curve dominated by the trailing-edge separation alone is not large enough to be clearly noticeable.

4.3.4 Drag

As it was mentioned earlier, it was not possible to predict the total drag on the aerofoil. But using the modified pressure distribution found with the potential flow, it is possible to predict the pressure drag. Figure 4.9 shows the pressure drag and the total drag measurements for the 18% aerofoil. The predicted pressure drag is also shown and falls within the experimental error. Here also the uncertainty region is represented by the cross on the figure. The drag measurements for the 10% aerofoil are also shown on the figure. It can be noticed that the difference between the total drag and the pressure drag is much less in the case of the 10% aerofoil than it is for the 18% aerofoil. This was expected since the surface area of the 18% aerofoil is larger than the 10% and the flow was also more turbulent on the 18% aerofoil than on the 10%.

For the 10% aerofoil the minimum drag is very close to the design incidence (2.0°). It is not the case for the 18% aerofoil. This is explained by the large region of separation present at design incidence for the 18% aerofoil. This trailing-edge separation greatly increases the drag. The minimum drag is found at an angle of attack for which a large leading-edge bubble is formed on the intrados of the aerofoil. Even though a large region of separation is present, this

72

configuration of the flow produces less drag than with a trailing-edge separation.
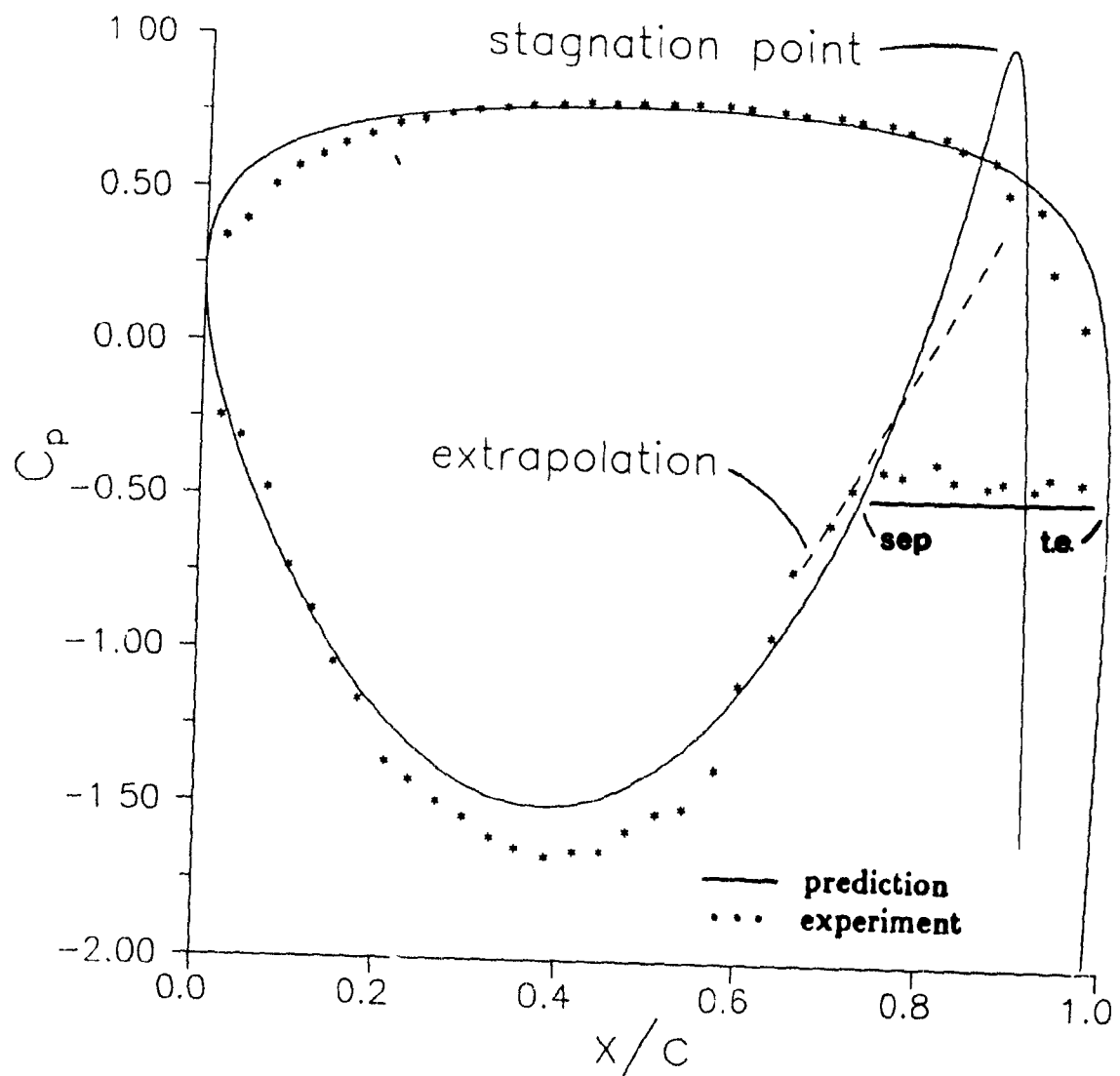
Figure 4.1: Measured pressure distribution with extrapolated part after separation compared with the present simulation
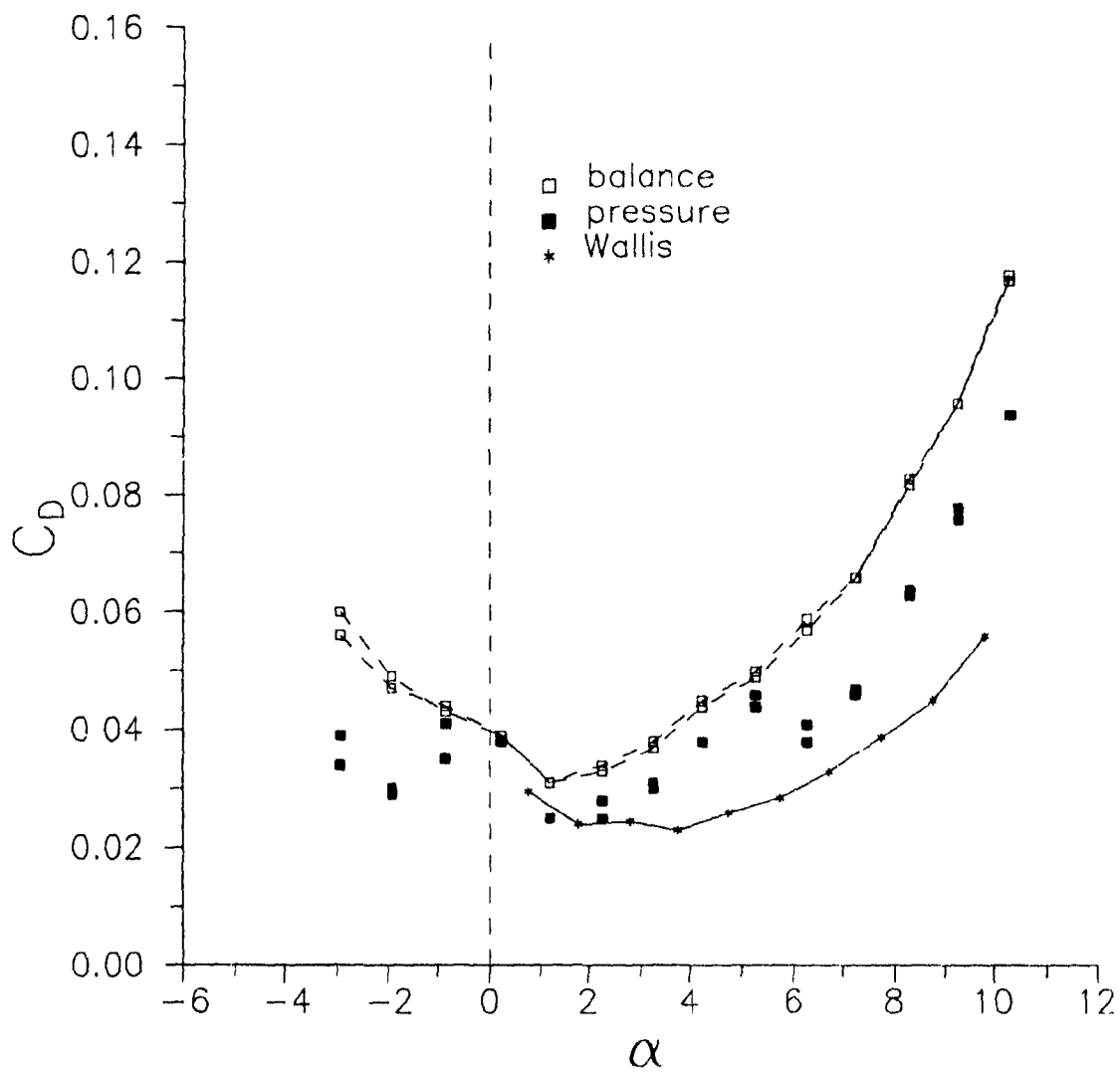
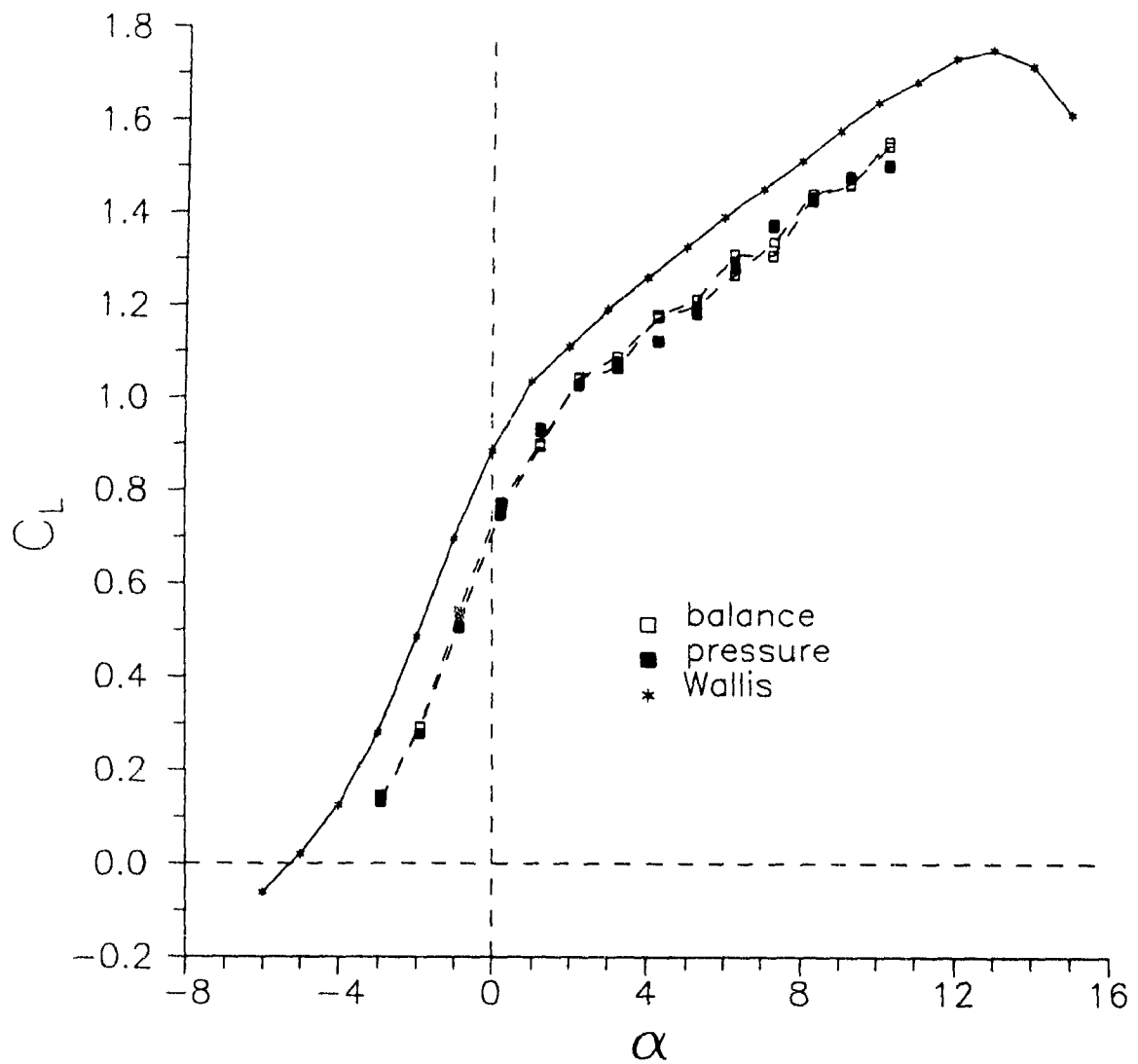Figure 4.2: Drag for the 10% circular-arc for a rounded leading-edge

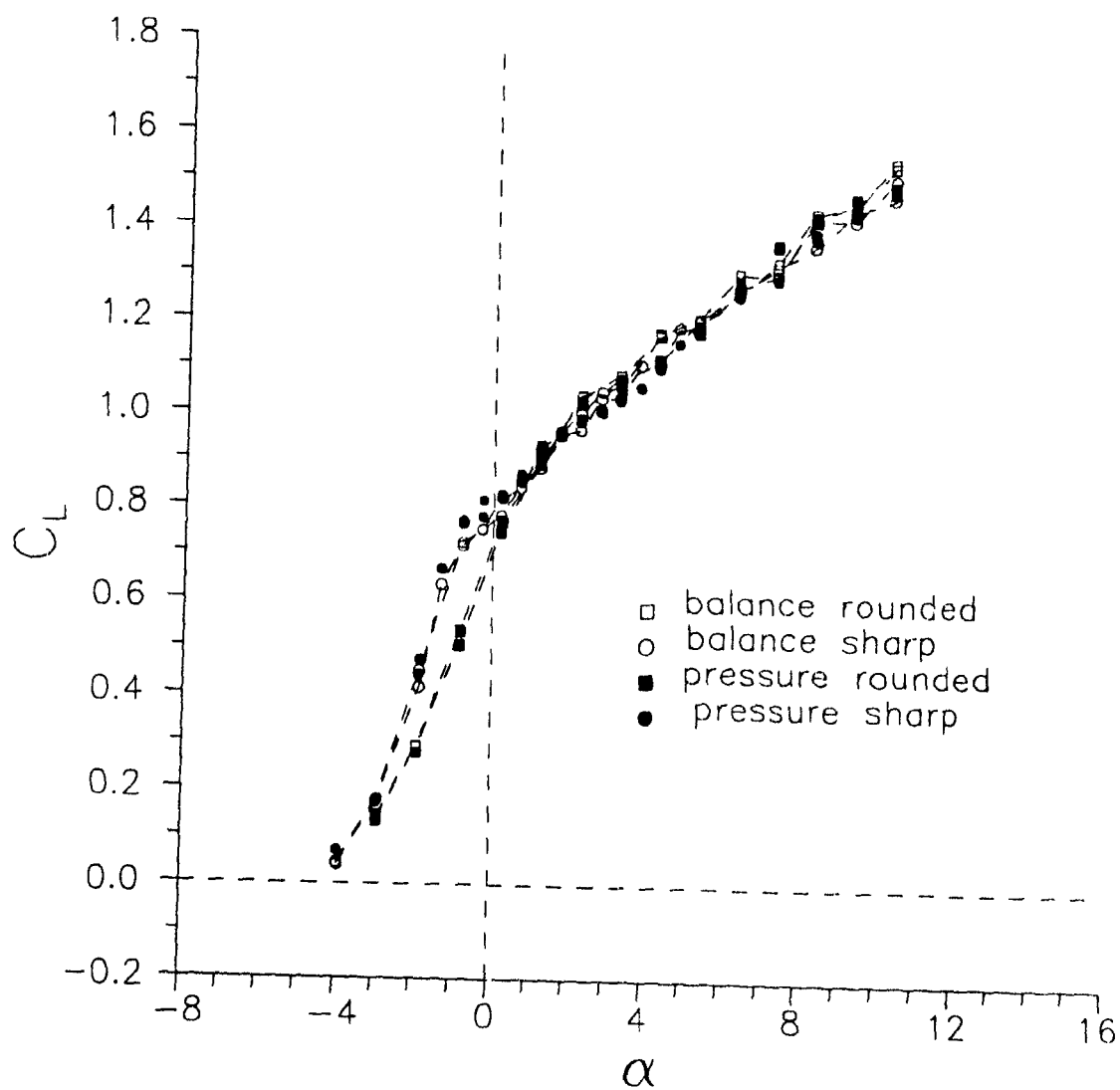Figure 4.3: Lift for the 10% circular-arc for a rounded leading-edge

Figure 4.4: Comparison between the lift obtained with a sharp and a rounded leading-edge for the 10% circular-arc
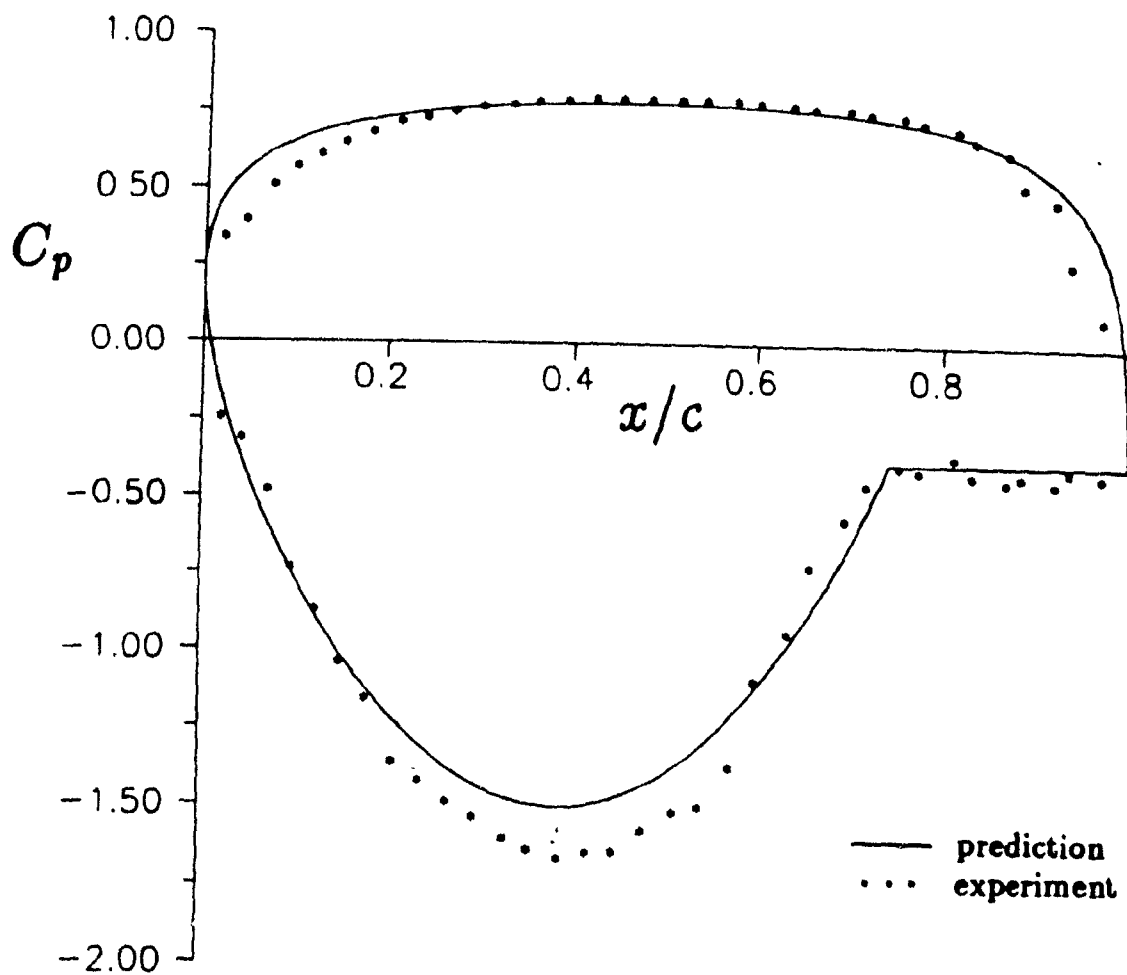
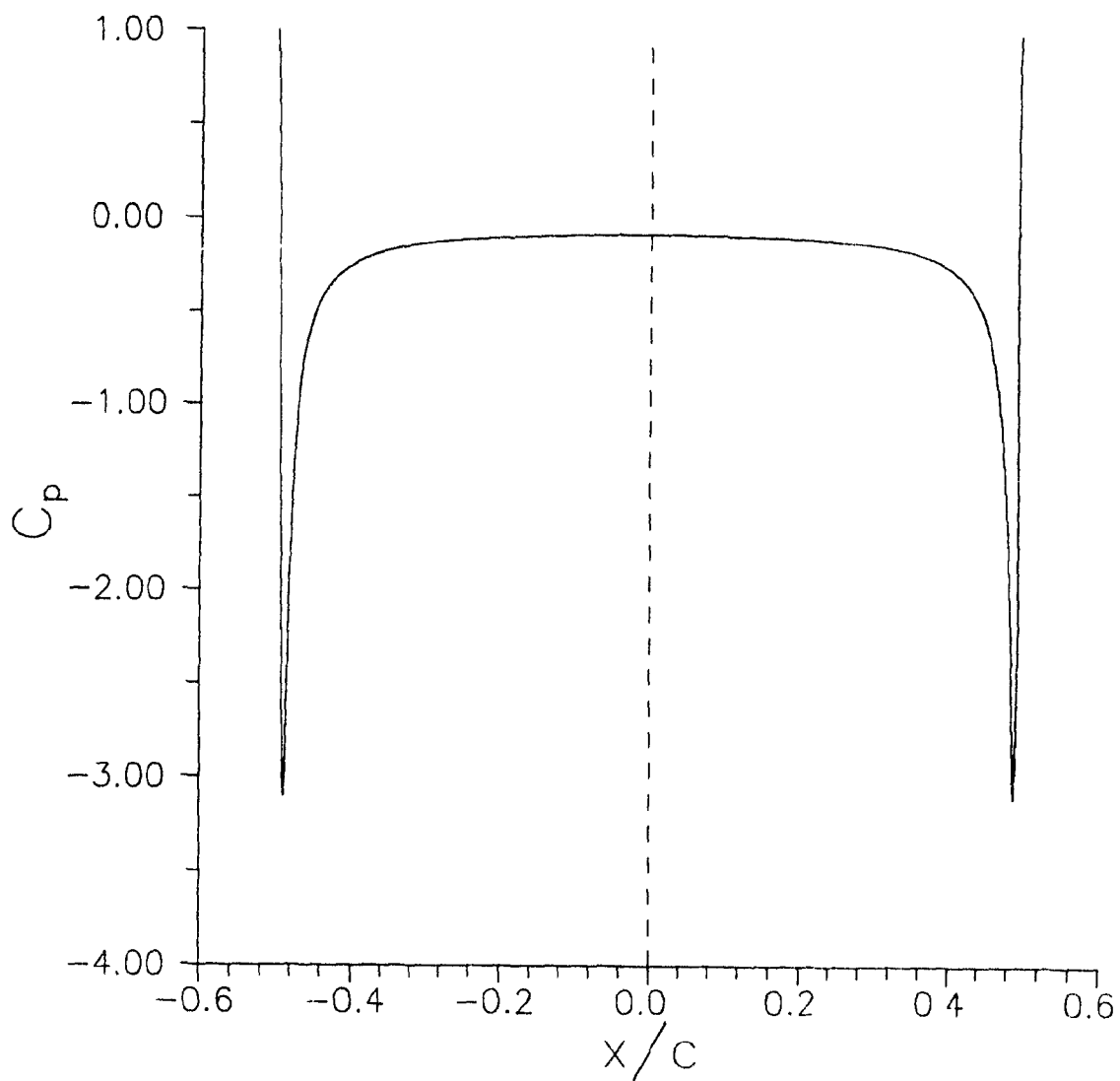Figure 4.5: Pressure distribution around the 18% aerofoil at $\alpha_d = 6.5°$

Figure 4.6: Pressure distribution around a slender Rankine oval; $t/C = 1/72$ and $\alpha = 0°$
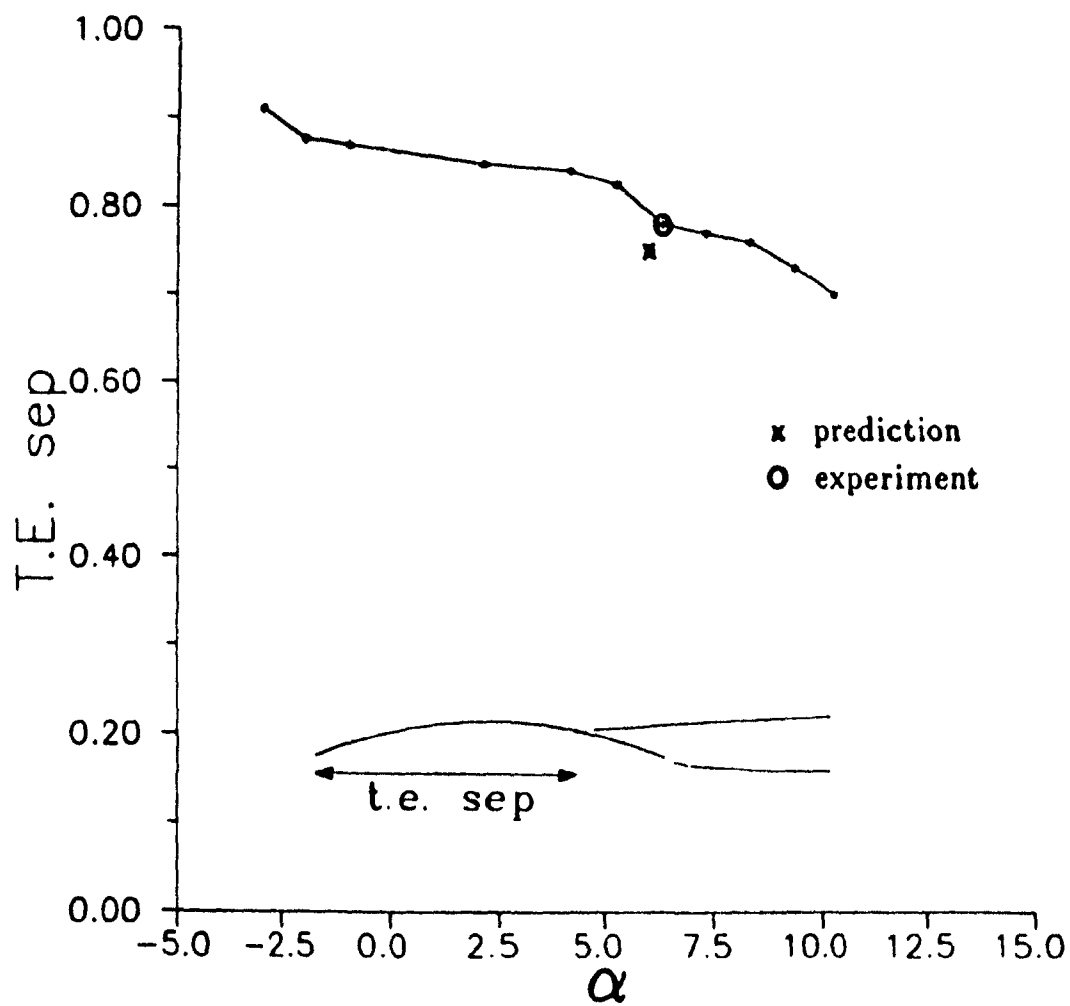
Figure 4.7: Trailing edge separation measured from the leading-edge *vs.* α for the 18% aerofoil. Comparison is made for the design incidence
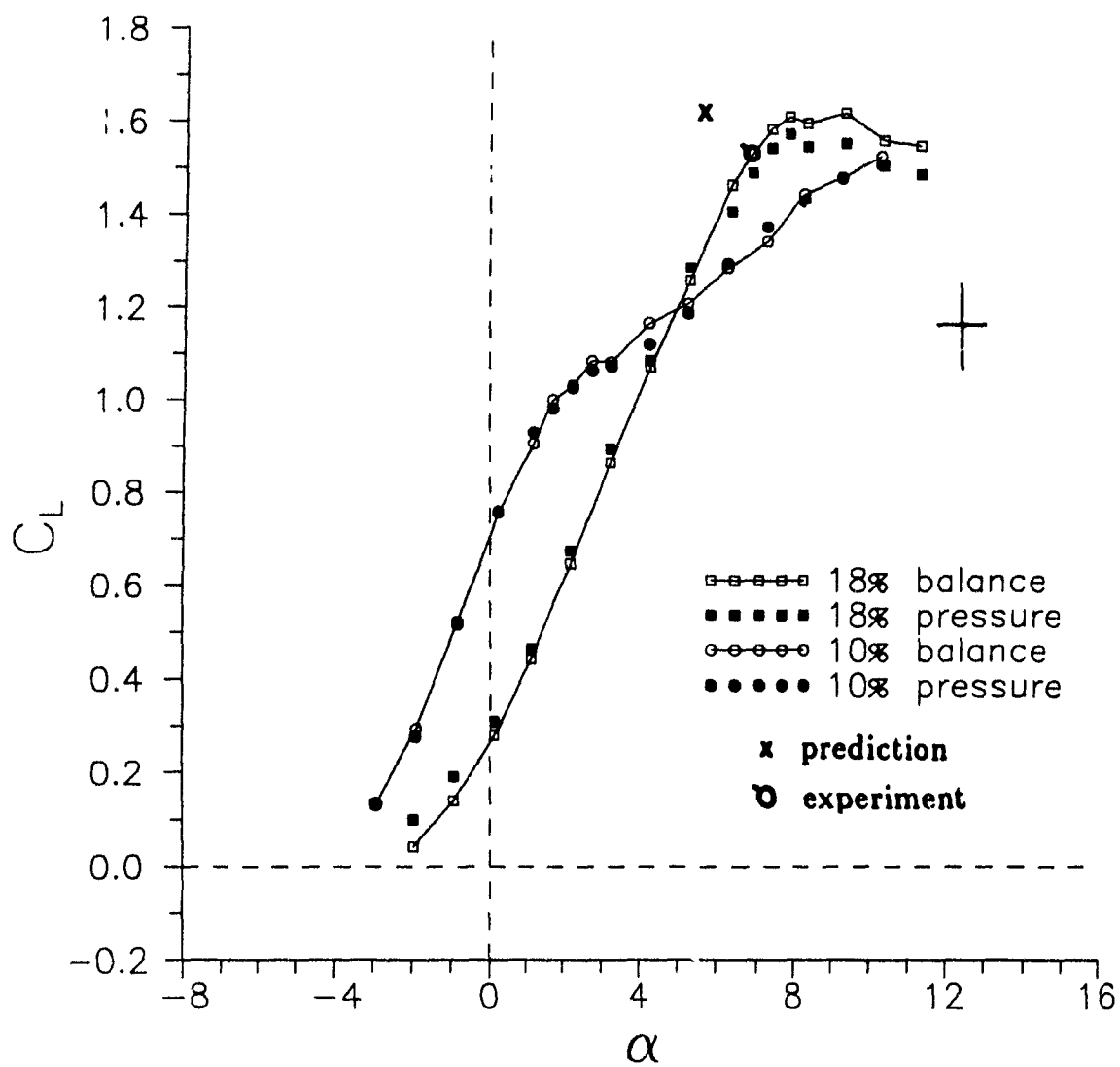
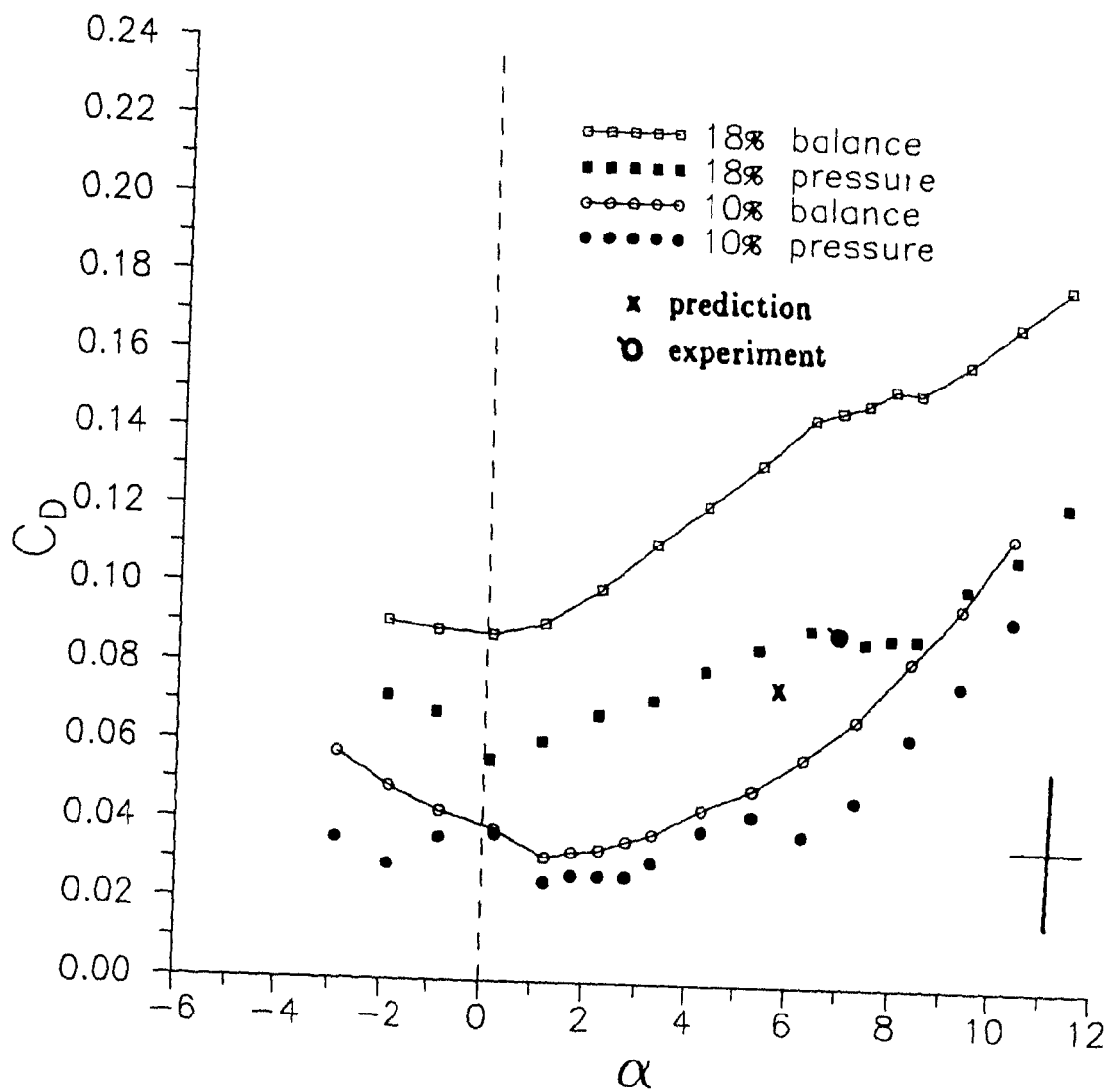Figure 4.8: Lift for the 10% and the 18% circular-arcs

Figure 4.9: Drag for the 10% and the 18% circular-arcs

Chapter 5

Conclusions and
recommendations

5.1 Conclusions

A theoretical model simulating the effect of a large separated wake on a circular-arc aerofoil has been developed. The model uses a point source implanted in the potential flow near the trailing-edge of the aerofoil to simulate the separated region. Four hypotheses, which serve as closure conditions, are used to make a realistic potential flow around the aerofoil. Those conditions are:

- the Kutta condition

- the design incidence condition

- the base pressure hypothesis

- the lift hypothesis

The last two of them use the result of a turbulent boundary-layer calculation, which finds the position of separation in the presence of separation itself. The theoretical model predicts the pressure distribution, the base pressure, the position of separation, the lift, the drag and the design incidence.

A series of experiments were conducted in a wind tunnel to measure all the results predicted by the theoretical model and guide its development. Two experimental aerofoils were tested. For a 10% cambered arc, some data was already available [19]. The comparison between the results of the two 10% aerofoils showed that the present experimental method gave sufficiently satisfactory agreement. Hence the predicted results obtained from the simulation of a turbulent flow separating over a circular-arc aerofoil of 18% camber at design incidence, is compared to the experimental results obtained in the present work. From this comparison and from the analysis of the theoretical model, the following conclusions can be drawn

- Sources are very good to simulate the essence of separation in the wake of an aerofoil [11]. Like a real separation region, they introduce the additional pressure gradient due to separation itself.

    - They simulate a pressure distribution around the aerofoil close to what is found on a real aerofoil.

    - They provide the appropriate pressure gradient for boundary-layer calculation to predict separation. (i.e. the boundary-layer calculation uses a pressure distribution that extends beyond the point of separation sought for.)

- With the four hypotheses used in the model, it is found that a point source is better than a distribution of sources to represent the separated wake of a circular-arc aerofoil of 18% camber and has the additional advantage of requiring one less boundary condition.

- The theoretical model is able to predict a point of separation and a corresponding base pressure because of the use of a boundary-layer calculation. It is believed to be an improvement on the model developed by Parkinson [11] where the position of separation and the base pressure are both prescribed.

- Predictions of lift, base pressure and separation point, design incidence and pressure drag are good.

- Predictions of lift and form drag are within 5% of the experimental results.

- This model is so far limited to constant density flows over aerofoils with trailing-edge separation only.

- This theoretical model compares very well with much more complex models using the time-averaged Navier-Stokes equations. It is relatively simple, fast and does not require very powerful computers. It therefore seems to have a place among the hierarchy of methods.

- Although the present theory has only been strictly justified for a circular-arc with 18% camber, it seems likely that the two additional conditions, namely the base pressure condition and the lift condition, will remain valid for cambers near 18%.

5.2 Recommendations

- A first recommendation would be to get more experimental test cases for circular-arc aerofoils, *i.e.* for other cambers.

- The circular-arc could be replaced by other aerofoils and the simulation could be done for a range of angles of attack, as long as there are no leading-edge separations.

- Data like the evolution of the momentum thickness and shape factor on the surface that leads to separation, should be measured and compared with the results obtained from the turbulent boundary-layer calculation.

- The combination of potential flow with sources, to represent the separated wake, and boundary-layer development calculations, to find the point of separation, should be used to simulate the flow over bluff bodies.

- The theoretical model should be extend to flows over two-dimensional sails with separation.

References

[1] Bradshaw, P., & Wong, F.Y.F., The reattachment and relaxation of a turbulent shear layer, *J. Fluid Mech.*, **52**, p.113 (1972)

[2] Güven, O., Farell, C. & Patel, V.C., Surface-roughness effects on the mean flow past circular cylinders, *J. Fluid Mech.*, **98**, p. 673 (1980)

[3] Head, M.R. & Patel, V.C., Improved entrainment method for the calculating turbulent boundary layer development, *ARC*, R&M No. 3643 (1970)

[4] Head, M.R., Entrainment in the turbulent boundary layer, *ARC*, R&M No. 3152 (1958)

[5] Maskew, B. & Dvorak, F.A., Investigation of separation models for the prediction of ClMAX, *AHS Paper* 77-33-01, (1977)

[6] Moffat, R.J., Describing the uncertainties in experimental results, *Exp. Thermal and Fluid Sci.*, **1**, p.3 (1988)

[7] Milne-Thomson, L.M., Theoretical aerodynamics, *Macmillan & Co.*, London (1948)

[8] Newman, B.G., Tse, M.C., Incompressible flow past a flat plate aerofoil with leading edge separation bubble, *Aero. J.*, Royal Aero. Soc., Feb (1992)

[9] Newman, B.G. & Low, H.T., Two-dimensional impervious sails: experimental results compared with theory, *J. Fluid Mech.*, **144**, p.445 (1984)

[10] Parkinson, G.V. & Jandali, T., A wake source model for bluff body potential flow, *J. Fluid Mech.*, **40**, p. 577 (1970)

[11] Parkinson, G.V. & Yeung, W., A wake source model for aerofoils with separated flow, *J. Fluid Mech.*, **179**, p. 41 (1987)

[12] Pope, A., Rae, W.H., Low speed wind tunnel testing, *Wiley*, New York (1984)

[13] Prandtl, L. & Tietjens, O.G., Applied Hydro- and Aero-Mechanics, *Dover Publications* (1934)

[14] Schlichting, H., Boundary Layer Theory, 7th ed., *McGraw-Hill*, New York (1987)

[15] Storm, P.V., A pressure instrument for measuring skin friction on rough walls, Master's thesis, Mech. Eng., McGill University (1991)

[16] Taylor, G.I., Air resistance of a flat plate of very porous material, *ARC*, R&M No. 2236 (1948)

[17] Thwaites, B., Incompressible Aerodynamics, *Clarendon Press*, Oxford (1960)

[18] Tse, M.C., Overall effects of separation on thin aerofoils, Ph. D. thesis, Mech. Eng., McGill University (1991)

[19] Wallis, R.A., Wind tunnel tests on a series of circular arc plate aerofoils, *ARL*, Aero Note 74, (1946)

[20] Wygnanski, I., Newman, B.G., General description and calibration of the McGill 3 ft. x 2 ft. wind tunnel, *Internal report Ae4*, Mech. Eng., McGill University (1961)

[21] Young,A.D., Boundary Layers, *Blackwell Scientific Publications*, Oxford (1989)